ORIGINAL PAPER

The age and composition of the pre-Cenozoic basement of the Jalisco Block: implications for and relation to the Guerrero composite terrane

Victor A. Valencia · Kevin Righter ·
Jose Rosas-Elguera · Margarita López-Martínez ·
Marty Grove

Abstract The Jalisco Block is thought to be part of the Guerrero terrane, but the nature and age of the underlying crystalline basement are largely unknown. We have collected a suite of schists, granitoids, and weakly metamorphosed marine sediments from various parts of the Jalisco Block including Atenguillo and Ameca, Mascota and San Sebastián, Cuale, Puerto Vallarta, Punta Mita, Yelapa, and Tomatlán. The schists range in age from 135 to 161 Ma, with many exhibiting Proterozoic and Phanerozoic zircon ages. The granitoids range in age from 65 to 90 Ma, and are calc-alkaline compositionally—similar to granitoids from the Puerto Vallarta and Los Cabos batholiths. The Jalisco granitoids also experienced similar uplift rates to granitoids from the regions to the north and south of the Jalisco Block. The marine sediments yield a maximum depositional age of 131 Ma, and also contain a significant zircon population with ages extending back to the Archean. Granitoids from this study define two age groups, even after the effects of thermal resetting and different closure temperatures are considered. The 66.8-Ma silicic ash flow tuff near Union de Tula significantly expands the extent of this Cretaceous–Paleocene age ash flow tuff unit within the Jalisco Block, and we propose calling the unit "Carmichael silicic ash flow tuff volcanic succession" in honor of Ian Carmichael. The ages of the basement schists in the Jalisco Block fully overlap with the ages of terranes of continental Mexico, and other parts of the Guerrero terrane in the south, confirming the autochthonous origin of the Jalisco Block rather than exotic arc or allochthonous origin. Geologic data, in combination with geochronologic and oxygen isotopic data, suggest the evolution of SW Mexico with an early 200–1,200-Ma passive margin, followed by steep subduction in a continental arc setting at 160–165 Ma, then shallower subduction by 135 Ma, and finally, emplacement of granitoids at 65–90 Ma.

V. A. Valencia
School of Environment, Washington State University,
Pullman, WA, USA

K. Righter (✉)
NASA Johnson Space Center, Mailcode KT,
Houston, TX 77058, USA
e-mail: kevin.righter-1@nasa.gov

K. Righter
Lunar and Planetary Institute, 3600 Bay Area Blvd.,
Houston, TX 77058, USA

J. Rosas-Elguera
Laboratorio Interinstitucional de Magnetismo Natural,
Universidad de Guadalajara, Guadalajara, Mexico

J. Rosas-Elguera
Centro Universitario de los Valles, Universidad de Guadalajara,
Ameca, Mexico

M. López-Martínez
Depto. de Geología, CICESE, Carretera Ensenada-Tijuana No
3918, Zona Playitas, 22860 Ensenada, Baja California, Mexico

M. Grove
Geological and Environmental Sciences, Stanford University,
Stanford, CA, USA

Introduction

The tectonic history of Mexico is dominated by magmatic belts accreted during several different periods of arc magmatism. The Guerrero terrane represents a major period of magmatism spanning the Mesozoic, and has a large extent from Sinaloa in northern Mexico to near Taxco in southern Mexico (Fig. 1). Detailed studies have resulted in models for the Guerrero terrane based on specific regions mostly in the eastern and central portions of the terrane (e.g., Centeno-García et al. 1993, 2008, 2011; Martini et al. 2011), but detailed investigations of the western portion of the Guerrero terrane still remain scarce (Centeno-García et al. 2008). In particular, the western part of the Guerrero terrane has been heavily studied with respect to young tectonism due to oceanic plate rifting and arc magmatism (Allan et al. 1991; Barrier et al. 1990; Ferrari et al. 1997; Ferrari and Rosas-Elguera 2000; Luhr et al. 1985; Lonsdale

1995; Luhr 1997; Rosas-Elguera et al. 1996, 1997; DeMets and Traylen 2000; Righter 2000). However, very little is known about the age or provenance of the basement lithologies in this region. Detailed study of the pre-Cenozoic basement units of this region could help to distinguish between the competing hypotheses of allochthonous (e.g., Dickinson and Lawton 2001) or an autochthonous (Centeno-García et al. 2008; Martini et al. 2011) origin for the Guerrero terrane.

The western part of the Guerrero terrane is comprised of the Jalisco Block (Rosas-Elguera et al. 1993; Allan 1986; Righter and Carmichael 1992; Righter et al. 1995), a fault-bounded crustal block at the western end of the Mexican Volcanic Belt (MVB) (Fig. 1). The basement lithologies within the Jalisco Block include Cretaceous to Early Cenozoic silicic ash flow tuff (54–114 Ma; Gastil et al. 1978; Wallace and Carmichael 1989; Righter et al. 1995; Rosas-Elguera et al. 1997), and co-eval or older plutonic rocks (Böhnel et al. 1992). The ages of the ash flow tuffs are in contradistinction to the Oligocene to Early Miocene (32–18 Ma) ash flow tuffs associated with the Sierra Madre Occidental to the north (Moore et al. 1994; Gastil et al.
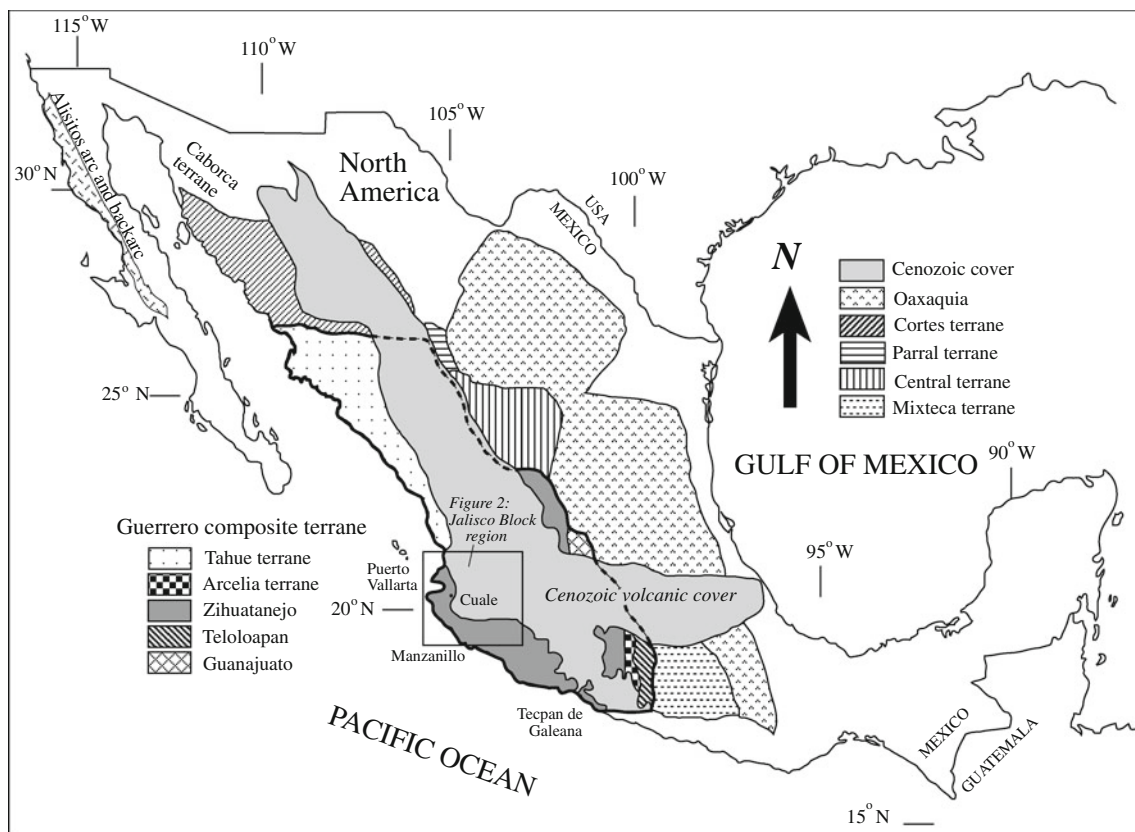
Fig. 1 Terrane map for most of Mexico, with the subterranes within the Guerrero composite terrane indicated on the *left hand legend* and outlined in a heavier border in the map. Older terranes to the north and east of Guerrero are indicated in *right hand legend*. Also shown is

the Cenozoic volcanic cover. The Jalisco Block is at the western end of the Guerrero terrane. Area of study for this project is outlined in the *rectangle* and enlarged in Fig. 2. Terrane map and boundaries are after Campa and Coney (1983) and Centeno-García et al. (2011)

Fig. 2 Sample locality and geologic map showing schist (*squares*), marine sediment (*diamond*), granitoid (*circles*), and silicic ash flow tuff (*stars*; Carmichael tuff volcanic succession; see text for discussion) localities from this study (Online Resource 2; Table S1). Also shown are Puerto Vallarta and the towns of Zacatongo, Amatlán de Cañas, Atenguillo, Talpa, San Sebastián, Mascota, Cuale, and Tomatlán. Samples Mas-808, Mas-433, Mas-427, Mas-607, LV-237, and LV-250 are silicic ash flow tuff samples from the studies of Righter et al. (1995) and Wallace and Carmichael (1989). Sample AUT-02 is a newly dated sample reported here. Information about additional Carmichael tuff samples is presented in the Online Resource 1 and 2. Sample KR-458 is just off the north edge of the map. Map assembled from data available from the Consejo de Recursos Minerales of Mexico (CRM) Geologic map scale 1:500,000
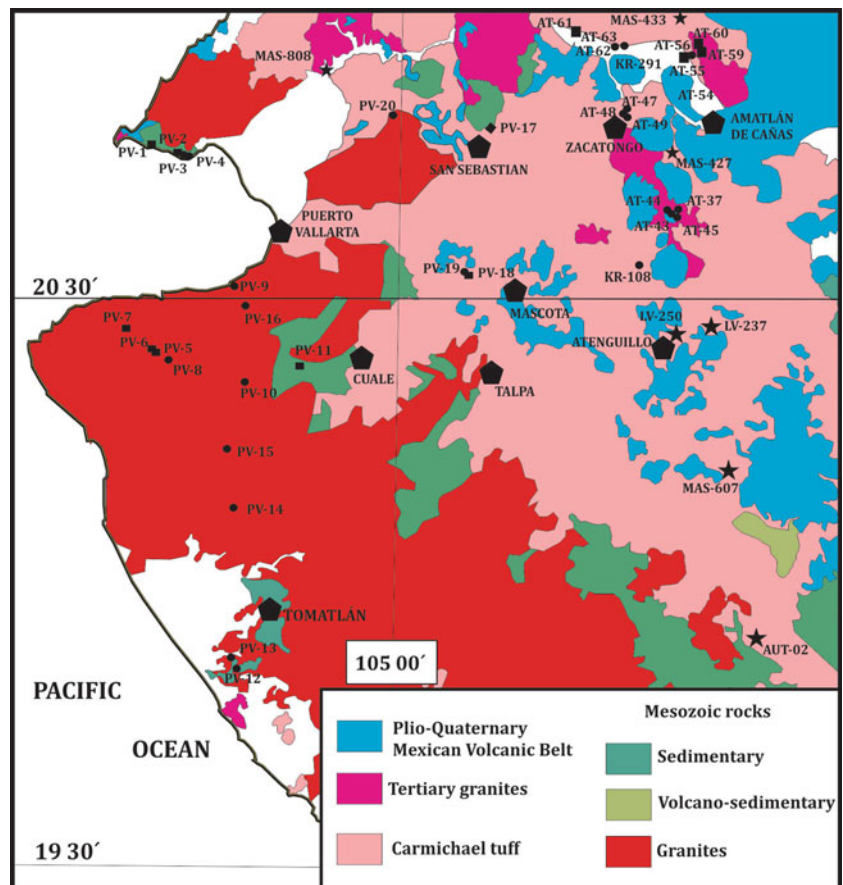
1978; McDowell and Keizer 1977; Aguirre-Diaz and McDowell 1991; Ferrari et al. 2007). Published dates of Gastil et al. (1978), Zimmerman et al. (1988), Köhler et al. (1988), Böhnel et al. (1992), and Wallace and Carmichael (1989) show that the transition from younger to older ash flow tuff units takes place north of the Ameca River Valley is abrupt, and is also roughly defined by the presence of Cretaceous plutons. The abrupt transition in the age of the ash flow tuffs indicates a tectonic origin, such as terrane accretion, uplift, or faulting. Although it may represent a terrane boundary (Sedlock et al. 1993; Ferrari et al. 2000; Spinnler et al. 2000), available paleomagnetic data show that both Baja California and southwest Mexico were immobile relative to the North American Plate from the mid-Cretaceous until initiation of the opening of the Gulf of California (e.g., Böhnel et al. 1992; Schaaf et al. 2000). The boundary may instead have been caused by uplift of the crust in response to subduction of the Rivera Plate and its predecessor, the Cocos Plate (Bandy and Hilde 1995; Dougherty et al. 2012).

We have collected a suite of magmatic, metamorphic, and marine sedimentary rocks from the basement of the Jalisco Block (Fig. 2), with a goal of defining several aspects of its relation to units within the Guerrero terrane. First, U–Pb zircon ages for these units allow comparison

to other regions of the Guerrero terrane to determine whether there are any significant differences or variations within the terrane. Second, ages and compositions of magmatic plutons from several belts are compared to previous work to evaluate the idea that there are discrete magmatic belts within the Jalisco Block (e.g., Zimmerman et al. 1988). Third, the areal extent and age of the Cretaceous to Paleocene silicic ash flow tuff volcanic units are discussed with respect to the Guerrero terrane. Fourth, O isotopes and U–Pb ages of zircons from plutonic rocks with low εNd values are analyzed to evaluate the possibility that there is a slice of Precambrian crust beneath the Jalisco Block (e.g., Schaaf et al. 2000, 2003). And finally, all the data are synthesized to consider the question of whether evidence from the western part of the Guerrero terrane favors a distal or local origin of the magmatic arcs making up the Guerrero terrane (e.g., Busby 2004).

Sampling

Field photos, petrographic thin section images, modal analyses, and sample locations for many of the rocks that described below appear in Online Resource 1 and 2.

Table 1 XRF analyses for major (wt%) and trace (ppm) elements

Rock	AT-37 Diorite	AT-48 Porph. Grtd.	AT-55 Phyllitic schist	AT-56 Grtd.	AT-59 Mica schist	AT-61 Schist	AT-62 Basalt	AT-63 Grtd.	KR-108 Grtd.	KR-458 Grtd.
SiO_2	61.14	59.69	55.60	54.25	41.65	70.19	50.80	65.01	69.45	65.73
TiO_2	0.81	0.79	0.77	0.74	0.88	0.30	1.82	0.61	0.52	0.58
Al_2O_3	16.06	18.43	15.63	17.61	14.28	14.45	16.59	15.32	13.93	15.05
FeO*	4.63	5.15	7.47	6.61	10.07	3.57	8.88	4.87	3.16	4.16
MnO	0.14	0.09	0.13	0.15	0.17	0.03	0.16	0.09	0.06	0.06
MgO	2.14	2.51	4.63	6.05	20.54	1.05	6.36	2.82	0.98	1.72
CaO	8.03	5.48	7.65	5.94	7.89	0.32	7.97	2.46	2.22	3.26
Na_2O	1.98	3.70	5.78	4.93	0.97	2.34	3.57	2.48	2.89	3.23
K_2O	0.77	2.62	0.28	1.43	0.07	5.55	1.29	4.25	5.02	3.98
P_2O_5	0.18	0.17	0.19	0.19	0.15	0.09	0.52	0.13	0.10	0.13
Sum	95.87	98.61	98.13	97.91	96.65	97.88	97.96	98.05	98.33	97.89
LOI (%)	1.43	1.89	0.88	1.89	4.93	1.48	0.65	3.65	0.84	1.41
Ni	20	10	28	45	623	8	96	9	9	8
Cr	39	14	73	177	1,291	4	147	9	5	10
Sc	21	19	28	32	32	19	25	15	10	12
V	111	125	194	190	235	13	208	119	64	80
Ba	193	739	81	968	8	895	482	597	837	812
Rb	55	116	5	38	0	154	15	200	296	195
Sr	504	476	233	276	22	63	541	266	183	314
Zr	153	208	117	106	59	323	222	188	345	220
Y	20	25	18	19	15	47	32	21	47	30
Nb	7.8	6.4	4.8	4.3	4.0	15.6	18.9	5.9	10.3	9.2
Ga	20	20	14	15	15	25	20	16	15	16
Cu	137	29	61	10	55	2	34	34	40	14
Zn	35	74	42	85	93	73	98	55	50	51
Pb	10	10	2	3	1	19	6	9	17	14
La	20	20	19	8	7	39	26	20	39	27
Ce	47	46	32	27	17	85	54	47	82	59
Th	8	10	2	2	0	12	3	17	36	25
Nd	18	22	14	15	10	40	29	21	41	29

Rock	AT-291 Grtd.	PV-3 Grtd.	PV-6 Schist	PV-7 Schist	PV-10 Grtd.	PV-12 Grtd.	PV-13 Grtd.	PV-14 Grtd.	PV-16 Grtd.	PV-18 Schist
SiO_2	63.17	63.75	74.11	69.11	75.46	69.84	70.54	73.99	67.15	48.56
TiO_2	0.63	0.618	0.177	0.640	0.156	0.296	0.400	0.237	0.570	0.875
Al_2O_3	15.98	16.55	13.89	15.14	12.97	15.03	14.35	13.81	15.72	17.20
FeO*	4.93	4.66	1.88	3.58	1.29	2.18	2.06	1.48	4.28	8.55
MnO	0.09	0.079	0.045	0.050	0.012	0.086	0.041	0.051	0.071	0.219
MgO	2.31	1.59	0.34	1.48	0.28	0.51	0.87	0.49	1.16	3.35
CaO	4.75	2.72	2.02	1.65	2.08	1.99	1.82	1.82	3.92	6.33
Na_2O	3.23	4.37	3.15	2.57	3.10	4.28	3.76	3.95	3.93	3.29
K_2O	2.86	3.21	3.94	3.59	3.48	4.39	4.63	3.29	2.23	3.03
P_2O_5	0.13	0.193	0.054	0.127	0.032	0.092	0.089	0.065	0.178	0.627
Sum	98.07	97.74	99.59	97.94	98.86	98.70	98.55	99.18	99.21	92.03
LOI (%)	1.60	2.04	–	–	–	–	–	–	–	7.70
Ni	10	3	2	10	1	3	10	2	2	12
Cr	10	9	8	41	7	4	18	5	6	11
Sc	17	10	8	13	8	4	4	3	10	21

Table 1 continued

Rock	AT-291 Grtd.	PV-3 Grtd.	PV-6 Schist	PV-7 Schist	PV-10 Grtd.	PV-12 Grtd.	PV-13 Grtd.	PV-14 Grtd.	PV-16 Grtd.	PV-18 Schist
V	117	73	15	81	15	12	37	19	55	199
Ba	661	1,249	1,027	739	1,085	1,387	1,140	1,363	1,112	3,630
Rb	119	95	130	155	109	136	162	85	79	91
Sr	383	562	134	142	98	371	273	284	328	525
Zr	179	220	104	202	98	209	209	110	244	119
Y	25	19	33	32	59	17	15	11	25	21
Nb	6.9	7.2	7.1	11.1	4.9	10.3	9.8	7.3	9.6	12.7
Ga	19	19	16	19	15	17	15	16	21	18
Cu	7	4	1	18	1	4	11	2	3	53
Zn	57	87	45	71	8	35	25	39	76	85
Pb	9	9	31	26	14	27	13	18	11	3
La	8	24	28	31	29	31	42	26	38	19
Ce	31	51	53	63	56	61	74	48	75	41
Th	11	5	12	12	14	15	18	9	8	4
Nd	18	22	25	32	28	21	25	17	31	20

Schists

The schists were sampled in five different places in the Jalisco Block (Fig. 2). First, at the north end of the Atenguillo valley and along the road across the Sierra Ahuacatlán, two schists were sampled: AT-55, a phyllitic schist and AT-59, a mica schist close to the contact with granitoid AT-60. Along the newer road between Amatlán de Cañas and Uzeta, AT-61 was collected, a chalcopyrite-bearing quartzofeldspathic schist with well-developed centimeter-scale crenulation texture. Second, schist outcrops were sampled near Punta Mita, in a roadcut near the shoreline just east of the Destiladeras restaurant (PV-2); contact with the granitoid is preserved here as well. Third, south of Puerto Vallarta and through the town of El Tuito toward Chacala well-folded schists were sampled (PV-5, 6; medium grained quartzofeldspathic schist with muscovite and 1–2 cm quartz-rich bands), as well as a fourth very well-preserved (fresh) mica schist near the town of Yelapa (PV-7). The fifth locality is in the mining region of Cuale, along the road into the mining area—dark and distinctly foliated schist outcrops along the road here near Rancho El Aguacate (PV-11; same as Stop 6 of Schaaf et al. 2003).

Granitoids

Granitoids occur mainly in the SW part of the Jalisco Block, but we collected samples from as broad a region as possible including the Atenguillo and Amatlán de Cañas valleys, Tomatlán and Puerto Vallarta, Punta Mita, El Tuito, and Cuale areas (Fig. 2). The Atenguillo granitoids (AT-38 to -45) include samples from the river valley

below the town of Tio Cleto, from just north of the town of Zacatongo (AT-47 to -54), and from the Ameca River valley and north toward Uzeta (AT-56, 63). The Punta Mita granitoid was collected from along the coast near the Destiladeras restaurant (PV-3), and then, also along the road back to the east near Cruz de Juanacaxtle (PV-4). A coarse-grained, hornblende-bearing granitoid was collected between Chacala and El Tuito (PV-8). A granitoid sample was collected from along the road into the Cuale mining area (stop 3 of Schaaf et al. 2003) and is a very fresh biotite-bearing granitoid (PV-10). Samples from Tomatlán (PV-13) and closer to Puerto Vallarta (PV-9, 14, 15, 16) are from roadcuts near these cities; PV-9, 14, and 16 were especially unaltered and fresh. Finally, granitoid was also collected from near the town of Mascota; PV-19 is heavily weathered, while PV-20 is coarse grained with large quartz, pink feldspar, and greenish hornblende.

Marine turbiditic sedimentary rocks

Marine sedimentary rocks are described by Lange and Carmichael (1991) near San Sebastián. We collected one sample from a steep roadcut along the road between Mascota and San Sebastián (PV-17; Fig. 2). This sequence contained 5–10 cm bedding of calcareous siltstone, with an SE dip of 50°; some areas exhibit folding. A second marine sedimentary rock sample was collected from an outcrop N of the city of Mascota (PV-18; Fig. 2). This sequence contains alternating bands that are also deformed in some areas; it is likely a low-grade phyllitic schist rather than undeformed sedimentary rock.

Table 2 ICP-MS analyses for trace elements (ppm)

Rock	AT-37 Diorite	AT-48 Porph. Grtd.	AT-55 Phyllitic schist	AT-56 Grtd.	AT-59 Mica schist	AT-61 Qtzfldsp. schist	AT-62 Basalt	AT-63 Grtd.	KR-108 Grtd.	KR-458 Grtd.
La	18.4	18.6	16.3	14.0	4.3	38.5	23.7	17.7	38.3	25.7
Ce	36.2	38.3	29.7	25.8	10.1	75.9	49.3	36.9	78.9	53.8
Pr	4.5	4.7	3.5	3.1	1.4	8.8	6.2	4.4	9.5	6.5
Nd	18.6	20.0	14.6	13.2	6.9	35.5	27.1	17.9	37.5	26.1
Sm	4.36	5.04	3.43	3.51	2.28	8.74	6.78	4.17	8.72	6.25
Eu	1.17	1.26	1.13	1.13	0.77	1.23	2.09	0.89	0.90	0.99
Gd	3.80	4.76	3.17	3.38	2.40	8.22	6.40	3.73	7.52	5.53
Tb	0.63	0.78	0.53	0.54	0.43	1.43	1.01	0.63	1.30	0.93
Dy	3.61	4.60	3.20	3.28	2.62	9.20	6.09	3.85	7.77	5.58
Ho	0.75	0.94	0.64	0.67	0.54	1.90	1.19	0.77	1.57	1.11
Er	1.99	2.52	1.76	1.80	1.49	5.24	3.11	2.21	4.26	3.01
Tm	0.28	0.37	0.26	0.26	0.21	0.78	0.45	0.32	0.62	0.46
Yb	1.72	2.27	1.60	1.64	1.38	4.90	2.73	2.06	3.74	2.74
Lu	0.27	0.35	0.26	0.25	0.22	0.78	0.42	0.31	0.57	0.43
Ba	186	703	77.0	925	6.3	876	461	563	804	787
Th	8.2	10.8	4.6	2.7	1.0	13.4	1.8	19.8	38.4	26.1
Nb	7.1	6.1	3.9	3.8	2.8	15.9	18.5	5.8	10.2	8.5
Y	20.1	25.5	17.2	17.5	13.8	48.4	31.5	20.8	46.4	30.8
Hf	4.11	5.15	2.79	2.42	1.45	8.42	5.04	3.80	8.23	6.29
Ta	0.47	0.50	0.29	0.29	0.23	1.12	1.18	0.55	0.96	0.87
U	3.75	2.98	0.94	0.82	0.27	3.36	0.56	4.89	10.15	8.21
Pb	9.2	8.4	2.1	2.3	1.0	18.5	5.8	9.5	16.1	14.8
Rb	51.7	105.0	4.4	35.3	0.5	142.7	13.7	182.4	268.7	181.8
Cs	10.2	12.9	0.2	0.7	0.1	5.1	1.6	4.5	7.3	6.6
Sr	486.5	447.3	226.6	264.6	23.3	58.7	530.6	245.0	166.9	296.2
Sc	20.6	19.8	28.7	35.4	32.5	22.2	26.7	15.0	10.6	12.4
Zr	144.8	185.7	107.4	98.0	51.1	297.3	209.9	111.7	276.0	201.8

Rock	AT-291 Grtd.	PV-3 Grtd.	PV-6 schist	PV-7 schist	PV-10 Grtd.	PV-12 Grtd.	PV-13 Grtd.	PV-14 Grtd.	PV-16 Grtd.	PV-18 schist
La	10.9	28.1	26.0	32.4	30.5	31.9	44.2	26.6	37.1	19.0
Ce	26.1	52.4	54.0	66.0	59.7	64.4	77.0	47.4	71.9	38.1
Pr	3.6	6.1	6.7	8.2	7.6	6.2	8.2	5.1	8.5	4.8
Nd	16.4	22.3	25.2	31.6	29.5	21.1	26.7	16.9	31.3	19.8
Sm	4.43	4.55	6.01	7.13	7.03	3.70	4.35	2.94	6.32	4.63
Eu	0.91	1.15	0.72	1.41	0.76	0.87	0.87	0.67	1.50	1.52
Gd	4.17	3.82	5.36	6.42	7.56	2.87	3.19	2.21	5.37	4.49
Tb	0.73	0.61	0.91	1.05	1.39	0.46	0.48	0.34	0.83	0.69
Dy	4.52	3.55	5.53	6.16	9.04	2.68	2.65	1.88	4.92	4.01
Ho	0.94	0.71	1.19	1.19	1.98	0.56	0.52	0.38	0.99	0.80
Er	2.56	1.89	3.43	3.21	5.58	1.56	1.43	1.07	2.59	2.12
Tm	0.38	0.26	0.52	0.47	0.82	0.24	0.21	0.16	0.36	0.30
Yb	2.43	1.66	3.37	2.88	4.85	1.53	1.35	1.05	2.23	1.93
Lu	0.37	0.26	0.52	0.44	0.76	0.25	0.20	0.17	0.34	0.31
Ba	646	1,254	1,036	757	1,116	1,421	1,185	1,388	1,126	3,600
Th	11.4	5.4	11.2	12.1	13.1	14.9	18.0	8.9	7.3	2.8
Nb	6.4	6.7	6.8	10.6	5.1	9.7	9.4	6.9	8.8	11.9

Table 2 continued

Rock	AT-291 Grtd.	PV-3 Grtd.	PV-6 schist	PV-7 schist	PV-10 Grtd.	PV-12 Grtd.	PV-13 Grtd.	PV-14 Grtd.	PV-16 Grtd.	PV-18 schist
Y	25.8	18.0	31.4	30.7	56.6	17.1	14.1	10.5	24.7	20.2
Hf	4.82	5.16	3.48	5.39	3.33	5.50	5.71	3.13	5.78	2.79
Ta	0.65	0.41	0.64	0.94	0.60	0.81	0.84	0.64	0.44	0.70
U	4.87	1.10	2.54	3.35	3.40	3.75	4.57	1.72	1.43	1.20
Pb	10.1	9.1	30.1	24.5	12.8	26.2	12.8	15.2	9.9	3.4
Rb	111.5	93.7	129.6	154.8	112.2	136.5	163.6	85.8	78.5	87.7
Cs	2.1	1.5	4.2	12.2	3.0	2.2	3.1	2.1	2.7	3.6
Sr	365.0	569.6	138.1	146.7	103.1	387.7	284.9	290.6	336.6	528.4
Sc	16.8	9.8	7.5	12.5	7.5	2.9	3.9	3.1	11.5	20.7
Zr	156.8	210.4	103.5	194.7	94.9	214.9	206.0	107.7	229.3	117.6

Basaltic dike

AT-62 is a piece of a basaltic dike that was collected along the road between Amajaquillo and San Valentin. The dike cuts across the basement schist here and therefore may yield the age of the first extension in this area. It was primarily collected for Ar–Ar dating.

Silicic ash flow tuff

A sample of silicic ash flow tuff from near Unión de Tula (Fig. 2) was collected for dating purposes and to compare to the various Cretaceous to Paleocene-aged ash flow tuffs from other parts of the Jalisco Block, such as near Tepic, Atenguillo, Atemajac, and Amatlán de Cañas (Gastil et al. 1978; Wallace and Carmichael 1989; Righter et al. 1995; Rosas-Elguera et al. 1997; Frey et al. 2004).

Methods

Whole rock XRF and ICP-MS

Major and trace elements (including Gd, U, and Th) were measured using a Rigaku 3370 wavelength dispersive X-ray spectrometer (XRF) and inductively coupled plasma mass spectrometry (ICP-MS; see below) at Washington State University (WSU) (Tables 1, 2). Samples for fused bead analysis were prepared by mixing 3.5 g of sample with 7.0 g $Li_2B_4O_7$ flux, and then, fusing the mixture into glass disks. Standards used in these analyses were a set of USGS standards (PCC-1, BCR-1, BIR-1, DNC-1, W-2, AGV-1, GSP-1, G-2, and STM-1; see Johnson et al. 1999). Loss on ignition measurements (Table 1) were performed by heating approximately 2 g of rock powder in a

Table 3 Summary of U–Pb zircon analyses of samples from this study

Sample	Location	Age	Uncertainty
Granitoids			
PV-3	Destiladeras beach	92.1	1.4
PV-4	Cruz de Juanacaxtle	78.3	1.1
PV-8	Chacala/El Tuito	80.9	1.2
PV-9	S. of Puerto Vallarta	82.1	1.3
PV-10	Cuale	160.4	2.5
PV-13	S. of Tomatlàn	84.9	1.4
PV-14	32 km N. of PV-13	83.8	1.3
PV-15	15 km N. of PV-14	80.2	1.4
PV-16	Mismaloya	80.6	1.1
PV-19	Near Mascota	79.4	1.1
PV-20	Mile marker 58 on road to Mascota	80.5	1.2
AT-37	Tio Cleto diorite	71.8	2.0
AT-44	Tio Cleto granite	69.6	2.0
AT-45	Tio Cleto granite	60.7	1.8
AT-47	Zacatongo granite 3,121 ft el.	59.4	1.7
AT-54	Zacatongo granite 1,924 ft el.	61.2	1.5
AT-56	Ahuacatlàn granodiorite	133.2	1.8
AT-63	Uzeta granite	64.0	1.4
Schists			
PV-2	Schist	152.0	6.1
PV-5	Schist	161.9	3.5
PV-6	Schist	159.4	5.9
PV-7	Schist	246.6	7.2
PV-17	Phyllitic schist	138.9	3.7
PV-18	Phyllitic schist	145.5	5.2
AT-59	Ahuacatlàn mica schist	134.2	3.1
AT-60	Ahuacatlàn amphibolite	134.9	2.6
AT-61	Uzeta quartzo-feldspathic schist	162.8	4.0

All errors are at the 2-sigma level, and include random and systematic uncertainties

Schist ages represent average zircon ages from individual samples that make up the peaks in Fig. 7, as presented in Online Resource 4 (Table S2)

Table 4 Ar–Ar whole rock analyses of samples from Union de Tula and Atenguillo region (AT 37 and AT 62: $J = 0.0036385 \pm 0.0000052$; AUT 02: $J = 0.0045095 \pm 0.0000275$)

Run no.	Grains	Power (W)	$^{40}\text{Ar*}/^{39}\text{Ar}_K$	1σ	Age (Ma)	1σ	% $^{40}\text{Ar*}$	$^{40}\text{Ar}/^{36}\text{Ar}$	$^{37}\text{Ar}_{Ca}/^{39}\text{Ar}_K$
AT-37 summary									
1	2	2.8	9.18	0.07	59.3	0.4	93.8	4,725.6	0.36
2	2	3.1	9.39	0.08	60.6	0.5	94.2	5,063.9	0.24
3	2	4.0 (max)	9.69	0.06	62.5	0.4	69.1	956.7	0.24
4	3	4.0 (max)	9.34	0.03	60.3	0.2	95.0	5,858.5	0.25
5	3	4.0 (max)	9.55	0.04	61.6	0.2	83.1	1,748.6	0.13
6	3	2.3 (max)	9.56	0.05	61.7	0.3	86.9	2,262.9	0.96
7	3	6.0 (max)	9.39	0.05	60.6	0.3	77.2	1,297.8	0.23

Run no.	Power (W)	$^{40}\text{Ar*}/^{39}\text{Ar}_K$	1σ	Age (Ma)	1σ	% $^{40}\text{Ar*}$	$^{40}\text{Ar}/^{36}\text{Ar}$	$^{37}\text{Ar}_{Ca}/^{39}\text{Ar}_K$
Individual steps (3 to 7)[a]								
3a	0.5	9.84	0.15	63.5	1.0	47.1	559.0	0.32
3b	0.7	9.57	0.08	61.7	0.5	81.6	1,606.9	0.22
3c	1.1	9.52	0.05	61.5	0.3	88.7	2,691.9	0.17
3d	4.0	9.78	0.07	63.1	0.4	84.8	1,944.2	0.24
4a	0.5	9.25	0.05	59.7	0.3	89.7	2,870.8	0.27
4b	0.7	9.42	0.06	60.8	0.4	98.4	18,756.0	0.20
4c	1.1	9.45	0.06	61.0	0.4	99.2	38,272.6	0.24
4d	4.0	9.31	0.04	60.1	0.3	97.6	12,387.3	0.29
5a	0.3	9.69	0.18	62.5	1.1	48.7	576.5	0.18
5b	0.5	9.34	0.09	60.3	0.6	80.5	1,513.3	0.15
5c	0.7	9.49	0.06	61.2	0.4	88.7	2,613.8	0.11
5d	0.8	9.54	0.09	61.6	0.6	92.2	3,767.2	0.10
5e	1.1	9.79	0.04	63.1	0.2	99.2	37,391.7	0.11
5f	4.0	9.44	0.05	60.9	0.3	91.3	3,381.8	0.19
6a	0.2	9.82	0.48	63.3	3.0	48.6	574.9	1.14
6b	0.4	9.61	0.11	62.0	0.7	86.8	2,234.2	0.53
6c	0.7	9.55	0.06	61.6	0.4	93.3	4,435.6	0.35
6d	1.1	9.51	0.04	61.4	0.3	97.2	10,480.4	0.44
6e	2.3	9.52	0.09	61.5	0.6	91.6	3,498.3	3.33
7a	0.5	9.46	0.13	61.0	0.8	59.6	731.8	0.26
7b	0.9	9.31	0.04	60.1	0.3	89.3	2,759.8	0.16
7c	6.0	9.41	0.04	60.8	0.3	88.9	2,668.8	0.29

Run no.	Grams	$^{40}\text{Ar*}/^{39}\text{Ar}_K$	1σ	Age (Ma)[b]	1σ	% $^{40}\text{Ar*}$	$^{40}\text{Ar}/^{36}\text{Ar}$	$^{37}\text{Ar}_{Ca}/^{39}\text{Ar}_K$
AUT-2 summary								
1	0.0247	8.71	0.58	69.5	4.6	38.8	483.2	0.17
2	0.4014	8.46	0.10	67.5	0.9	46.3	550.4	0.20

Run no.	Temp	$^{40}\text{Ar*}/^{39}\text{Ar}_K$	1σ	Age (Ma)	1σ	% $^{40}\text{Ar*}$	$^{40}\text{Ar}/^{36}\text{Ar}$	$^{37}\text{Ar}_{Ca}/^{39}\text{Ar}_K$
Individual steps (1 and 2)[c]								
1a	900	8.66	0.41	69.1	3.2	62.2	781.1	0.05
1b	1,100	8.94	2.94	71.3	23.0	31.2	429.7	0.22
1c	1,350	8.91	4.12	71.1	32.2	9.0	324.7	1.32
2a	750	8.49	0.07	67.3	0.6	60.0	739.1	0.05
2b	900	8.39	0.09	66.5	0.7	60.9	755.6	0.10
2c	1,000	8.09	1.00	64.2	7.8	39.3	487.0	0.44
2d	1,100	8.12	1.25	64.4	9.7	32.1	435.2	0.71

Table 4 continued

Run no.	Temp	$^{40}\text{Ar*}/^{39}\text{Ar}_K$	1σ	Age (Ma)	1σ	% $^{40}\text{Ar*}$	$^{40}\text{Ar}/^{36}\text{Ar}$	$^{37}\text{Ar}_{Ca}/^{39}\text{Ar}_K$
2e	1,350	8.76	0.54	69.4	4.2	13.6	341.9	1.55

Run no.	Grains	Power (W)	$^{40}\text{Ar*}/^{39}\text{Ar}_K$	1σ	Age (Ma)	1σ	% $^{40}\text{Ar*}$	$^{40}\text{Ar}/^{36}\text{Ar}$	$^{37}\text{Ar}_{Ca}/^{39}\text{Ar}_K$
AT-62 summary									
1	1	1.6	0.54	0.15	3.54	1.01	25.9	398.6	4.8
2	1	2.0	0.44	0.06	2.86	0.42	33.1	441.5	2.0
3	2	3.8	0.45	0.08	2.97	0.53	15.4	349.5	2.5
4	2	4.8	0.60	0.05	3.93	0.35	22.5	381.5	1.6
5	3	1.5 (max)	0.44	0.07	2.90	0.44	26.0	399.6	4.2
6	3	1.5 (max)	0.57	0.08	3.72	0.51	38.4	479.7	3.0
7	5	6.0 (max)	0.49	0.04	3.23	0.25	30.0	422.4	2.6
8	5	6.0 (max)	0.53	0.04	3.48	0.25	29.0	416.5	3.0
9	5	6.0 (max)	0.44	0.05	2.91	0.35	21.6	376.9	3.0
10	5	6.0 (max)	0.46	0.03	2.99	0.23	31.4	430.7	2.3

Run no.	Power (W)	$^{40}\text{Ar*}/^{39}\text{Ar}_K$	1σ	Age (Ma)	1σ	% $^{40}\text{Ar*}$	$^{40}\text{Ar}/^{36}\text{Ar}$	$^{37}\text{Ar}_{Ca}/^{39}\text{Ar}_K$
Individual steps (5 to 10)[d]								
5a	0.8	0.35	0.09	2.28	0.61	14.6	345.9	2.4
5b	1.0	0.53	0.17	3.49	1.12	51.7	612.1	1.9
5c	1.5	0.58	0.11	3.80	0.73	80.9	1,548.4	8.9
6a	0.2	0.71	0.52	4.62	3.38	14.0	343.7	1.6
6b	0.5	0.64	0.08	4.18	0.52	42.0	509.7	2.1
6c	0.8	0.69	0.20	4.52	1.32	84.8	1,940.4	1.7
6d	1.5	0.39	0.13	2.55	0.84	43.9	527.2	5.2
7a	0.5	0.43	0.11	2.80	0.71	11.4	333.4	2.3
7b	0.9	0.51	0.05	3.36	0.32	56.6	681.1	1.7
7c	1.3	0.46	0.08	3.00	0.54	46.3	550.0	1.3
7d	6.0	0.56	0.06	3.66	0.38	67.2	890.0	4.6
8a	0.5	0.66	0.11	4.30	0.75	14.9	347.2	2.4
8b	1.3	0.60	0.04	3.91	0.27	60.7	751.5	1.5
8c	6.0	0.36	0.04	2.36	0.29	47.0	557.4	5.0
9a	0.3	0.15	0.21	0.95	1.39	2.3	302.5	1.4
9b	1.0	0.67	0.08	4.42	0.50	32.8	439.5	1.5
9c	1.5	0.39	0.10	2.53	0.64	48.3	571.7	1.9
9d	6.0	0.20	0.10	1.30	0.65	24.2	389.9	8.2
10a	0.3	0.33	0.23	2.19	1.51	6.3	315.5	1.1
10b	1.0	0.56	0.05	3.69	0.31	38.7	481.7	1.9
10c	1.5	0.34	0.06	2.24	0.42	45.1	538.1	1.6
10d	6.0	0.40	0.06	2.62	0.38	49.4	584.2	3.9

[a] Isochron age: 60.6 ± 0.2 Ma; $(^{40}\text{Ar}/^{36}\text{Ar})_i$ = 307 ± 6; MSWD = 4.1; n = 23

[b] Integrated age

[c] Isochron age: 67.2 ± 0.6 Ma; $(^{40}\text{Ar}/^{36}\text{Ar})_i$ = 297 ± 2; MSWD = 0.2; n = 8

[d] Isochron age: 3.10 ± 0.22 Ma; $(^{40}\text{Ar}/^{36}\text{Ar})_i$ = 302 ± 8; MSWD = 2.5; n = 26

preheated ceramic crucible to 1,000 °C for 2 h, and determining the resulting weight loss.

Additional trace element analyses (for all 14 naturally occurring rare earth elements (La through Lu) together with Ba, Rb, Y, Nb, Cs, Hf, Ta, Pb, Th, U, Sr, and Zr) were performed on a Sciex Elan model 250 ICP-MS equipped with a Babington nebulizer, water cooled spray chamber, and Brooks mass flow controllers at WSU's Geoanalytical

Table 5 Oxygen isotope analyses of zircon from this study

Sample	δ¹⁸O (‰ SMOW)	±1SD	n
PV8	6.1	0.4	4
AT55	6.7	0.5	4
PV10	9.0	0.6	5
AT56	5.7	0.7	5
AT63	7.5	0.3	5
PV18	8.1	0.4	3
PV9	7.4	0.3	3
SL2 (ALC*)	15.3	0.7	5
TEMORA	8.32	0.69	12

1SD one standard deviation, *ALC** Arizona LaserChron Center

Laboratory (with reproducibility (average of several replicate analyses/SD; Table 2)): La (1.86 %), Ce (1.20 %), Pr (0.98 %), Nd (1.75 %), Sm (2.07 %), Eu (1.92 %), Gd (1.13 %), Tb (1.12 %), Dy (1.33 %), Ho (1.53 %), Er (1.37 %), Tm (1.23 %), Yb (0.94 %), Lu (1.90 %), Ba (1.89 %), Th (9.50 %), Nb (2.6 %), Y (0.77 %), Hf (1.47 %), Ta (2.70 %), U (9.34 %), Pb (3.23 %), Rb (1.39 %), Cs (3.06 %), Sr (1.56 %), and Sc (3.46 %). Replicate analyses of sample AT-9 are also consistent with this reproducibility. Powdered sample was mixed with lithium tetraborate ($Li_2B_4O_7$) flux, fused, ground again, and dissolved in Teflon vials with internal standards of In, Re, and Ru. Working curves are constructed from a set of primary standards, and a series of secondary standards were run with the unknowns (Govindaraju 1994).

Zircon U–Pb ICP-MS laser geochronology

We processed ∼2–5 kg of each sample for zircons using standard heavy liquid and magnetic separation methods. A large fraction of the recovered zircons was mounted in epoxy resin and polished. Selection of zircons for analyses was made at random from ∼100 of the zircons mounted, and cores of grains were preferred to avoid possible metamorphic overgrowth or alteration; these could be identified using cathodoluminescence (CL) (Online Resource 3). The large majority of magmatic zircons analyzed exhibit various magmatic textures, such as complex growth zoning and sector zoning, with only a small number showing xenocrystic cores (e.g., Corfu et al. 2003; Online Resource 3). For magmatic samples ∼30 analyses were performed, analyzing tips and cores.

U–Pb geochronologic measurements were conducted in different sessions at the University of Arizona (U of A) and Washington State University (WSU). Operating procedures and parameters are described in Gehrels et al. (2008) and Chang et al. (2006), respectively. Zircon crystals were analyzed after CL imaging using 1″ polished epoxy grain

mounts with a micromass isoprobe multicollector ICP-MS equipped with nine Faraday collectors, an axial Daly collector, and four ion-counting channels coupled to an ArF excimer laser ablation system with an emission wavelength of 193 nm (U of A) and a ThermoFinnigan Element 2 single collector, double-focusing, magnetic sector ICP-MS coupled to a new wave Nd: YAG UV 213-nm laser (WSU). Laser spot size and repetition rate were 35–50 microns and 8 Hz, and 30 microns and 10 Hz, respectively. He and Ar carrier gases delivered the sample aerosol to the plasma. U–Pb diagrams were plotted using Isoplot 3.0 (Ludwig 2003). U–Pb zircon crystallization ages errors are reported using quadratic sum of the weighted mean error plus the total systematic error for the set of analyses (Valencia et al. 2005). A summary of the results are presented in Table 3, and a full table is available as Online Resource 4.

Ar–Ar

Three samples were analyzed for ⁴⁰Ar–³⁹Ar at the Geochronology Laboratory of the Departamento de Geología, Centro de Investigación Científica y de Educación Superior de Ensenada (CICESE). The samples were irradiated in the U-enriched research reactor of the University of McMaster, Hamilton, Ontario. Bulk samples AT-37 and AT-62 were irradiated for 30 MWh, with sanidine TCR-2 with reference age of 28.34 ± 0.28 Ma (Renne et al. 1998) as an irradiation monitor. Feldspar concentrate from sample AUT-02 was irradiated for 40 MWh with biotite CATAV 7-4 (89.13 ± 0.35 Ma: internal standard calibrated with hornblende hb 3gr at the University of Toronto and with hornblende MMhb 1 at the University of Nice) as an irradiation monitor. For samples AT-37 and AT-62, the VG5400 mass spectrometer online with the laser extraction system was used for the step-heating and one-step laser fusion experiments. Feldspar AUT-02 was step heated with a Modification Ltd. Ta-furnace online with an MS-10 mass spectrometer. The Ar isotopes were corrected for blank, mass discrimination and interference contributions from Ar isotopes derived from Ca, Cl, and K. The decay constants of Steiger and Jager (1977) were used in the age calculations and the equations presented in York et al. (2004) were used in all the straight-line calculations. A summary of the results are presented in Table 4.

Oxygen isotopes

The oxygen isotopic compositions of zircon crystals were measured within a 1″ inch polished epoxy zircon mount using the UCLA CAMECA ims 1270 ion microprobe. Samples were coated with ∼350 Å of gold. The ∼0.1–0.4-nA primary Cs⁺ beam was shaped into a spot ∼8–10 μm in diameter (usually in aperture illumination mode).
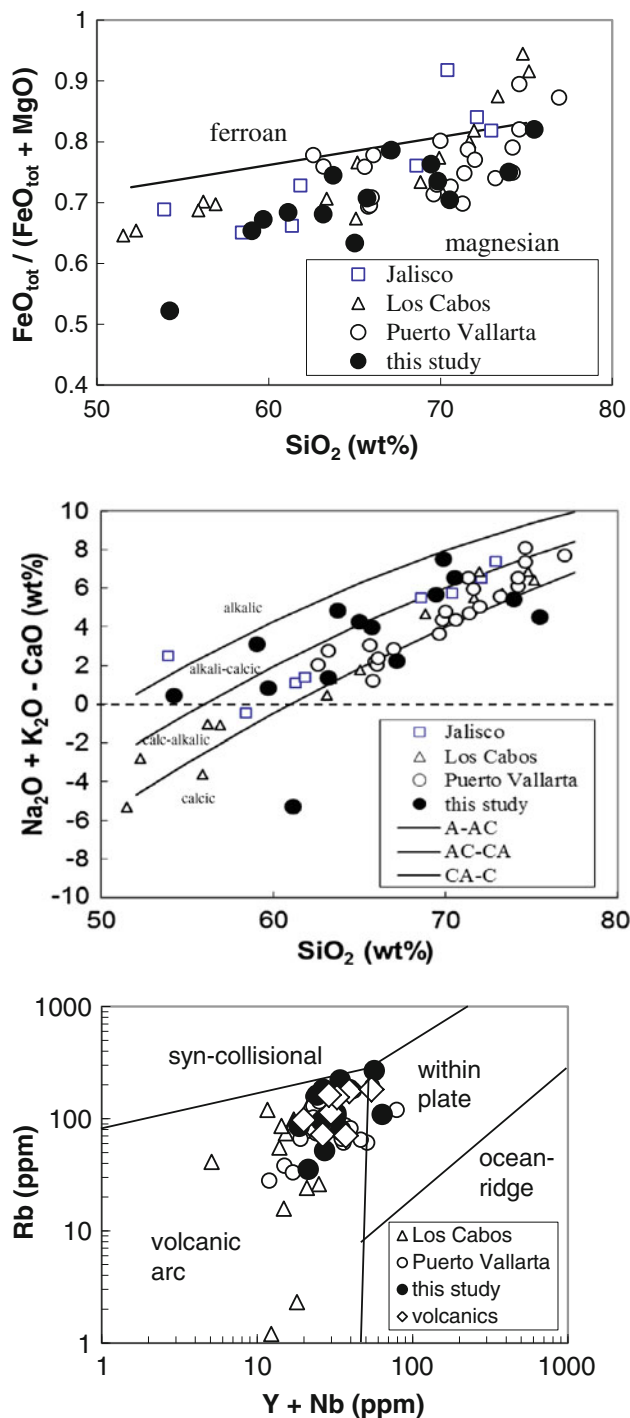
Fig. 3 Compositional diagrams for granitoids from this study, compared to those from Jalisco region (*squares*; Zimmerman et al. 1988), Los Cabos (*triangles*; Schaaf et al. 2000), and Puerto Vallarta batholith (*open circles*; Köhler et al. 1988; Schaaf 1990). Granitoid classification fields are from Frost et al. (2001) for **a** (ferroan vs. magnesian granitoids) and **b** (calcic, calc-alkalic, alkali-calcic, and alkali) and Pearce et al. (1984) for **c**

Charge compensation was achieved using a normal-incidence electron flood gun (Slodzian 1980). Low-energy (∼0–30 eV) negative secondary ions were measured at
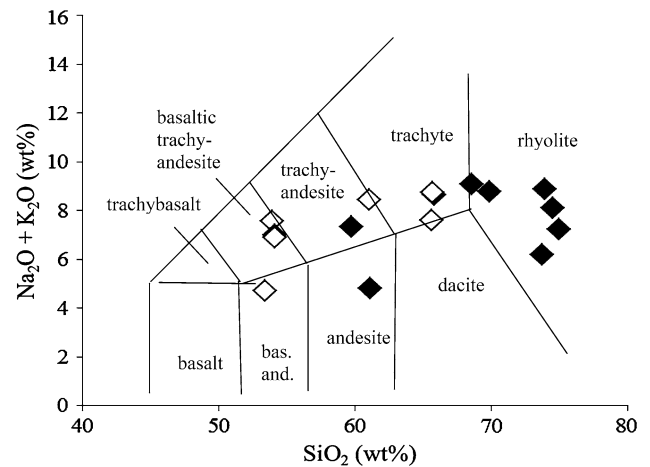
Fig. 4 Total alkalis versus silica diagram for the volcanic units of Cretaceous age in the Jalisco Block. Rock classification fields are from Le Bas and Streckeisen (1991). The *solid diamonds* are the silicic volcanic units (Carmichael tuff) from Righter et al. (2010), Wallace and Carmichael (1989, 1992) (LV-250), and KR-136 and PV-12 from this study. The *open diamond symbols* are the silicic dikes from the interior of the Jalisco Block reported by Frey et al. (2007). The Carmichael tuff units range from ∼55 to 75 % SiO₂ and range from subalkaline to alkaline

high-mass resolving power ($M/\Delta M$) of about 6,500. Measurements were made by magnetic peak switching through 25 cycles of counting $^{16}O^-$ for 3 s, and $^{18}O^-$ for 5 s. The secondary $^{16}O^-$ current was measured in a Faraday cup equipped with a Keithley 642 electrometer, and $^{18}O^-$ signals were pulse-counted on an electron multiplier with a deadtime of typical 20 ns. The analysis conditions typically yielded equivalent count rates of 20–40 million counts per second of $^{16}O^-$. Measured secondary ion intensities were corrected for background ($^{16}O^-$), and for deadtime ($^{18}O^-$). With the count rates employed in these experiments, the total magnitude of these corrections is small (<2 ‰), and thus, the additional uncertainties resulting from background and deadtime corrections are negligible (<0.1 ‰). Zircon R33 was used as a standard ($\delta^{18}O = 5.5$ ‰) to correct for instrumental mass fractionation. Isotopic data are reported in standard δ notation relative to Vienna SMOW (Table 5).

Results

Classification of granitoids and volcanic rocks

The granitoids studied here are classified as magnesian based on FeO$_{tot}$/(FeO$_{tot}$ + MgO) versus SiO₂, and as calc-alkaline granitoid based on Na₂O + K₂O–CaO versus SiO₂ (Fig. 3) as defined by Frost et al. (2001). There are a few samples that plot in the alkali-calcic field above the calc-alkalic, but this is observed in other arcs as well, where
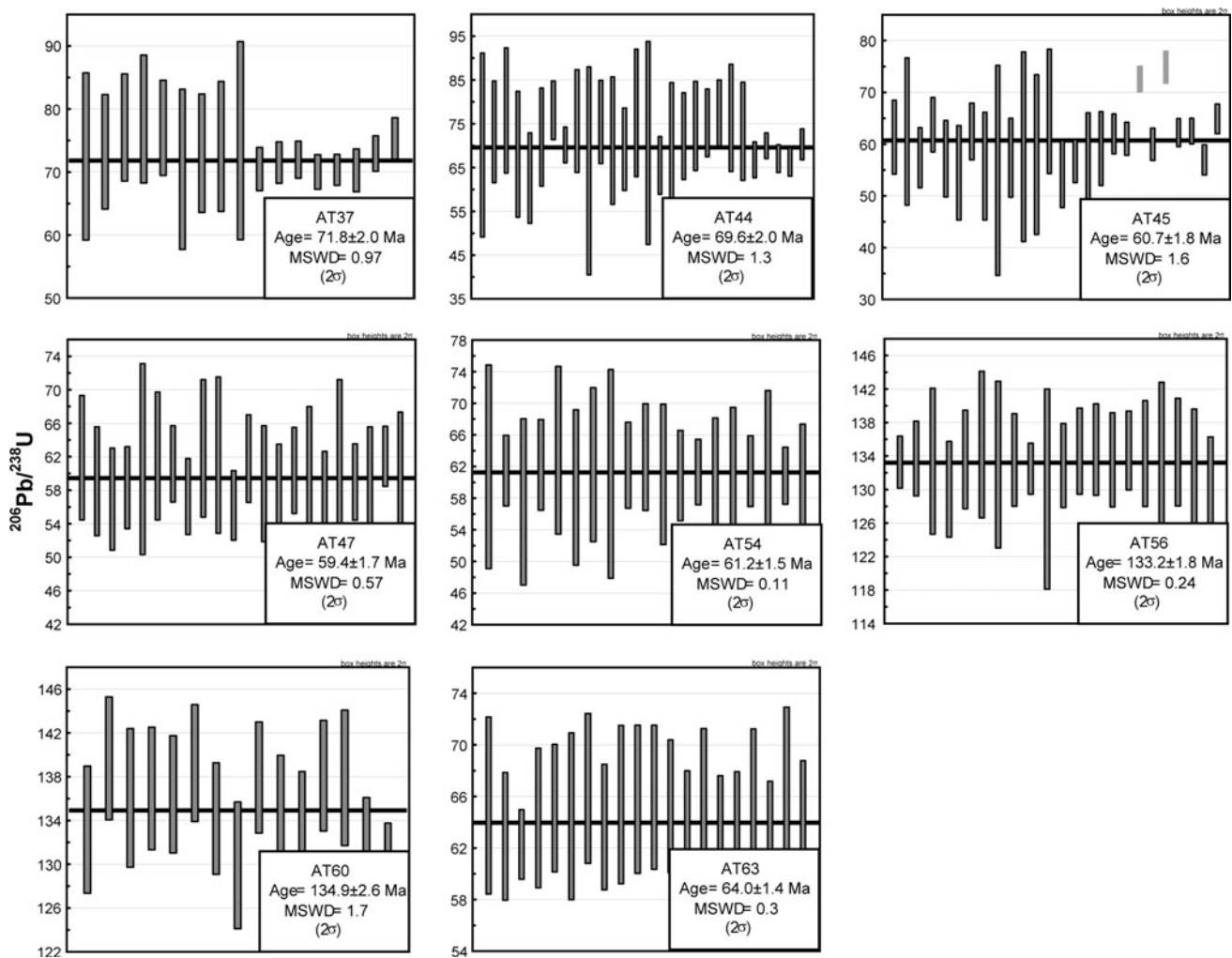
Fig. 5 U–Pb weight average plots for Atenguillo region samples. The weighted mean of many (*n*) individual analyses was calculated according to Ludwig (2003). The mean considers only the measurement or random errors (errors in $^{206}Pb/^{238}U$ and $^{206}Pb/^{204}Pb$ of each unknown). For most samples, the random error represents ∼1 %. Age of standard, calibration correction from standard, composition of common Pb, decay constant uncertainty are the other sources that contributed to the error in the final age determination. These uncertainties are grouped and are known as the systematic error, usually ∼2.0 %. The error in the age of the sample is calculated by adding quadratically the two components (random or measurement error and systematic error); all age uncertainties are reported at the 2-sigma level (2σ)

some alkali-calcic plutons occur inboard of the calc-alkalic arc (e.g., California; Frost et al. 2001). Similarly, consideration of the Rb versus (Y + Nb) diagram of Pearce et al. (1984) shows that the granitoids are classified as volcanic arc granitoids (Fig. 3). In fact, all the granitoids studied here, combined with others from central Jalisco (Zimmerman et al. 1988), Los Cabos (Schaaf et al. 2000), and the Puerto Vallarta batholith (Böhnel and Negendank 1988; Schaaf 1990), form a single coherent suite that is clearly of calc-alkaline, magmatic arc origin.

The ash flow tuff units found in the Jalisco Block are contemporaneous with the granitoids, and have been analyzed in a number of studies previously, including Wallace and Carmichael (1989, 1992), Frey et al. (2007), Righter

et al. (1995), and Righter et al. (2010). These samples range from andesite to rhyolite (and are hereafter referred to as "silicic") and are both alkaline and subakaline (Fig. 4). On an Rb versus (Y + Nb) diagram of Pearce et al. (1984), they also fall in the volcanic arc granitoids field, indicating a likely close relationship to the granitoids.

Zircon ages

The zircon ages for most of the granitoids fall into a restricted range between 59 and 92 Ma (Table 3), but there are a few older ages. In general, the Atenguillo samples yield the youngest ages at 59.4, 64.0, and 69.6 Ma for Tio Cleto (AT-44), Uzeta (AT-63), and Zacatongo (AT-47)
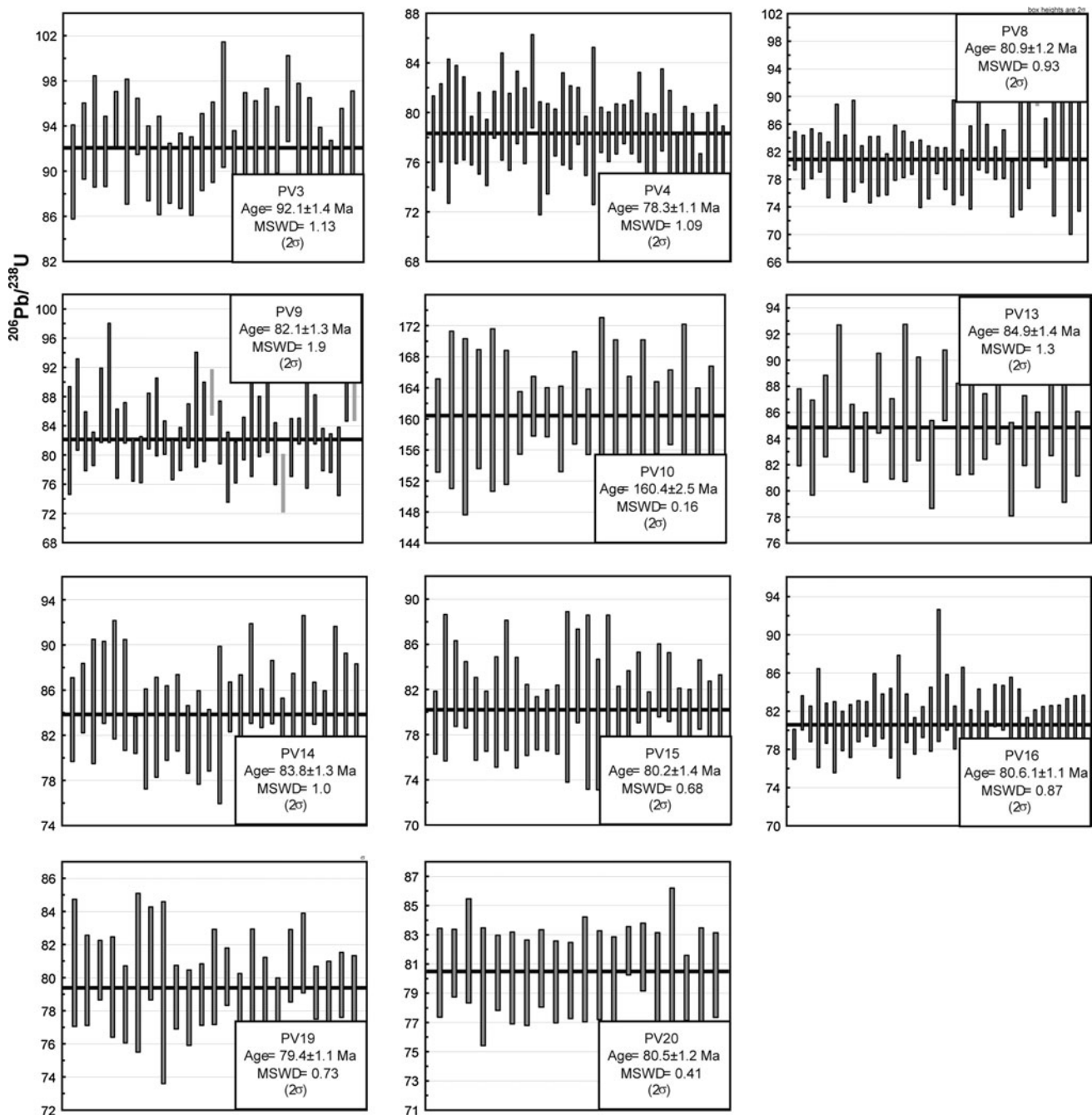
Fig. 6 U–Pb weight average plots for Puerto Vallarta region samples. Weighted means, error, and corrections are as explained in Fig. 5

granitoids, respectively (Fig. 5). The Atenguillo diorite (AT-37) yields an age of 71.8 Ma. In comparison, the samples to the west near Puerto Vallarta (Punta Mita, El Tuito, Mismaloya, Cruz de Juanacaxtle) yield slightly older ages from 78.3 to 92.1 (Fig. 6). The granitoid from Cuale (PV-10) yields an age of 160 Ma, much older than any of the other Jalisco Block granitoids, but comparable in age to several of the schist units (see below).

Detrital zircons from the marine sediments near San Sebastián (PV-17) and Mascota (PV-18) yield a range of

ages with most falling near 131 and 140 Ma, respectively. However, both of these samples yielded much older ages, as well, with peaks occurring in the Phanerozoic and Proterozoic (Fig. 7).

The schists also yield mainly Late Jurassic or Early Cretaceous ages with Ahuacatlán schist at 135 Ma (AT-59), Destiladera (PV-2), Punta Mita and El Tuito areas (PV-5, 6) at 157–166 Ma, the Uzeta schist (AT-61) at 164 Ma, and the Yelapa sample (PV-7) giving a much older 240-Ma peak age. In addition to this distribution of
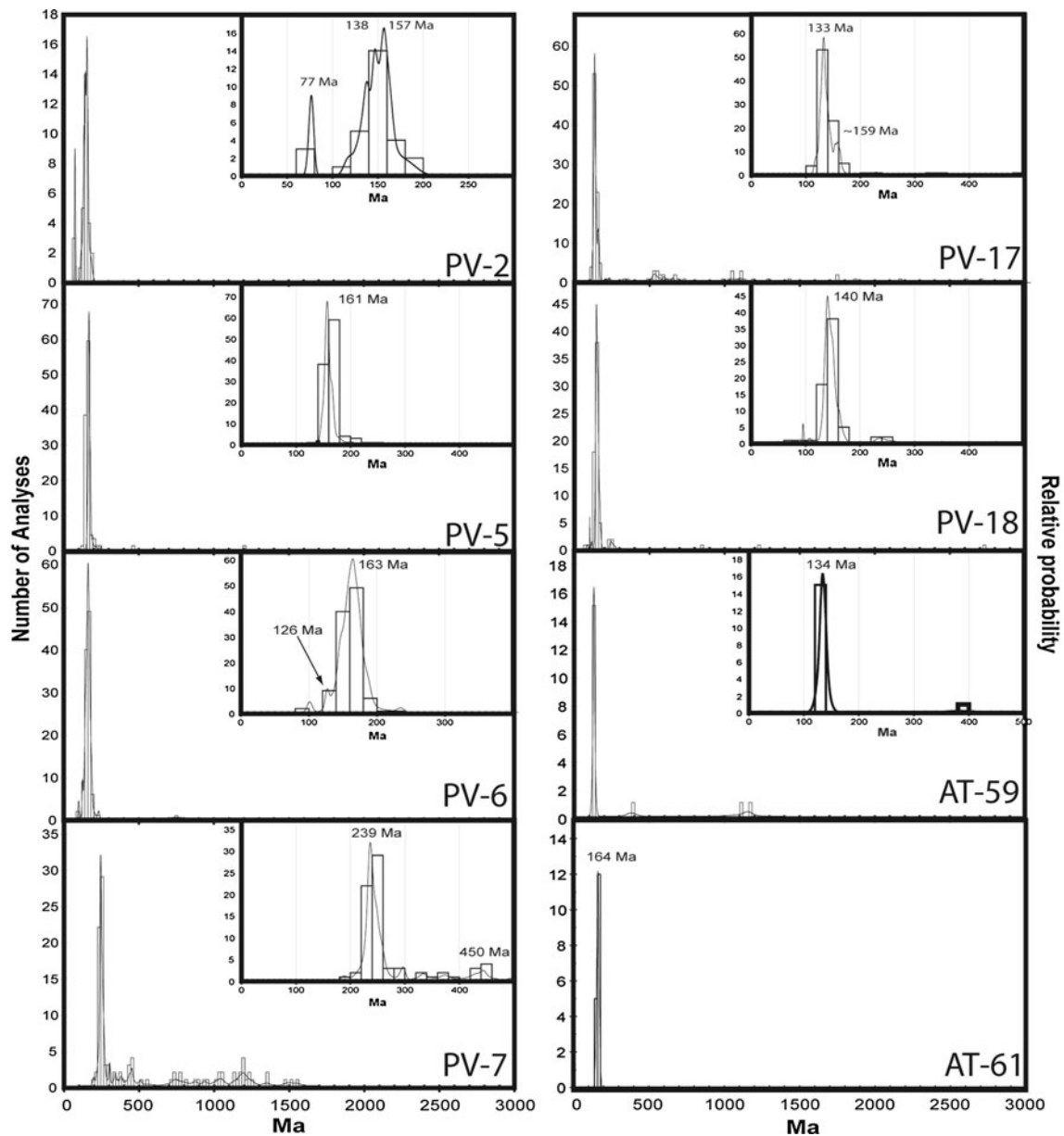
Fig. 7 U–Pb results for schists and metasediments from Puerto Vallarta and Atenguillo regions, including probability density plots

dominant ages, there are older zircon ages recorded in the Yelapa and Cuale samples, as old as 1.7 Ga (Fig. 8).

Ar results

For the Unión de Tula feldspar sample AUT-02, two step-heating experiments using the temperature controlled Ta-furnace were conducted. The argon isotopes were analyzed with the MS-10 mass spectrometer. A total of 8 fractions were collected, and these align in the $^{36}Ar/^{40}Ar$ versus $^{39}Ar/^{40}Ar$ correlation diagram to define an isochron age of 67.2 ± 0.6 Ma (Table 4; Fig. 9c).

The diorite at Tio Cleto (AT-37) was also dated using the $^{40}Ar–^{39}Ar$ method. Seven experiments were performed on sample AT-37, with the first two being one-step fusions on single grains. Between three and six steps were collected on five step-heating runs. Using equations given by York et al. (2004), the best isochron age for AT-37 is 60.6 ± 0.2 Ma (Table 4 and Fig. 9a, b).

For sample AT-62, ten experiments were performed, including four one-step fusions and six step-heating experiments with 3–4 fractions each. The 26 data points from the combined experiments scatter about the best straight line with an MSWD of 2.5; however, their

Fig. 8 Concordia diagrams for PV-2, PV-5, PV-6, PV-7, PV-11, PV-17, and PV-18 with inherited zircon ages
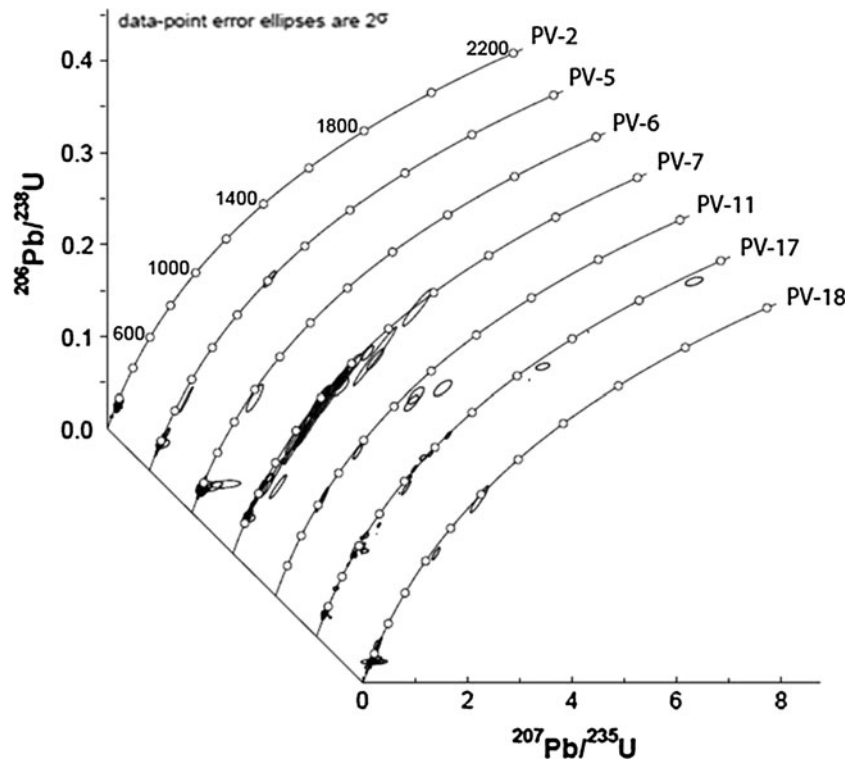
distribution along the line constrains the isochron age of 3.10 ± 0.22 Ma (Fig. 9d; Table 4). This age is very similar to the age of a basalt from near Santa Cruz de Camotlán studied and dated by Righter et al. (1995). Sample 403C from that study was collected near Cerro la Virgen and was dated at 3.38 ± 0.05 Ma (Righter et al. 1995).

Oxygen isotope results

Overall the granitoid and schist samples have $\delta^{18}O$ values that fall into a range between 5.7 and 9.0 per mil (Table 5). Two of the Atenguillo samples (AT-55 schist and AT-56 granitoid) and one Chacala/El Tuito granitoid sample (PV-8) have low values, below 7.0 per mil. AT-63 Uzeta granitoid and PV-9 Puerto Vallarta granitoid have values between 7.0 and 7.5 per mil. And PV-10 Cuale granitoid and PV-18 metasediment/schist from Mascota have the highest values of 9.0 and 8.1 per mil, respectively.

Discussion

Thermal and uplift history of the Jalisco Block

Some previous work has proposed the existence of plutonic belts of different ages in the Jalisco region of SW Mexico (e.g., Zimmerman et al. 1988). However, U–Pb zircon and Ar–Ar whole rock analysis of a sample from Atenguillo (AT-37) give two different ages indicating that the Ar–Ar

age may instead reflect a lower closure temperature. Our new ages, when combined with previous work, suggest that after correction for different closure temperatures of the U–Pb, Ar–Ar and Rb–Sr systems, there are indeed two groups of ages of plutonic rocks in the Jalisco Block region: the 80–91-Ma Puerto Vallarta batholith samples and the 59.4–64.0-Ma intrusive rocks in the Atenguillo and Ameca valleys.

Because of the different chronologic techniques that have been applied to plutonic rocks in this region, we can calculate cooling rates and compare them to other parts of western Mexico. Samples from several areas can provide constraints on the cooling history of the Jalisco Block. For example, for the Punta Mita granitoid, our U–Pb zircon age of 80 Ma (closure temperature of 900 °C; Cherniak and Watson 2001), combined with an K–Ar age (Zimmerman et al. 1988) for biotite of 67 Ma (280 °C closure temperature; Dodson 1973), yields a cooling rate of 48 °C/Ma. This calculation should be interpreted with caution because these two samples were not taken from the same outcrop; they only come from nearby each other. Further east, our diorite sample (AT-37) from the Tio Cleto locality in the Atenguillo region yields an Ar–Ar age of 60.6 Ma and a U–Pb zircon age of 71.8 Ma, thus, indicating a cooling rate of 34 °C/Ma. These cooling rates are similar to rates of 36–45°C/Ma measured for granitoids in the Los Cabos Batholith and for the Puerto Vallarta Batholith reported by Schaaf et al. (1995, 2000), but lower than those further south in the Acapulco and Oaxaca regions (∼100 °C/Ma;
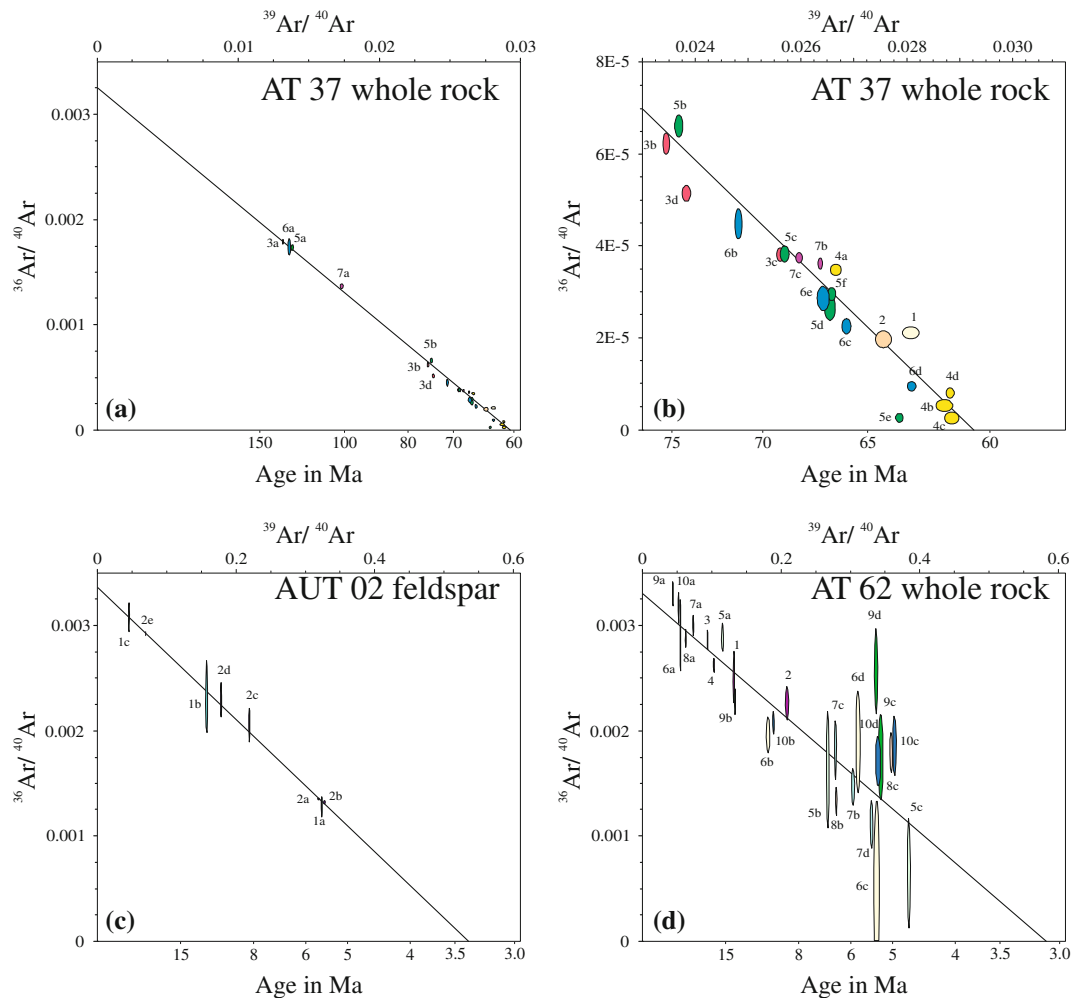
Fig. 9 ^{36}Ar/^{40}Ar versus ^{39}Ar/^{40}Ar correlation diagram for the samples analyzed. **a** Include one-step fusion and step-heating experiments performed on sample AT 37; **b** shows an enlargement of the region of the left-hand plot where most of the data plot. A total of 23 data points define (MSWD = 4.1) an isochron age of 60.6 ± 0.2 Ma; **c** two step-heating experiments of feldspar sample AUT-02, an isochron age of 67.2 ± 0.6 Ma is defined by 8 data points (MSWD = 0.2); **d** whole rock one-step and step-heating experiments of sample AT-62. The 26 data points from the combined experiments yield an isochron age of 3.10 ± 0.22 Ma (MSWD = 2.5)

Morán-Zenteno et al. 1996). The apatite fission track studies of the Los Cabos, Puerto Vallarta, and Manzanillo batholiths show that uplift in this region most likely occurred in Cretaceous to Eocene time followed by additional uplift in the Eocene to Oligocene timeframe (Calmus et al. 1999). Our results thus corroborate the previous work that has demonstrated moderate cooling rates (and high uplift rates) in the early Cenozoic.

Origin of granitoids and magmatic rocks

Previous work on the origin of granitoids within the Jalisco Block (Puerto Vallarta batholith; Köhler et al. 1988) suggested an important role for either altered oceanic crust melting or assimilation of continental crust based on Rb–Sr isotopes. Our oxygen isotopic results indicate a significant

role for continental crust, altered oceanic crust, and sediments, especially in the older Cuale granitoids (Fig. 10). This central role for crustal contamination is found in other Cordilleran granitoids (Tepper et al. 1993; Lackey et al. 2005; Valley et al. 2005). However, the elevated values for some of the Jalisco Block granitoids indicate that subducted marine sediments or altered oceanic crust must have played an important role in the genesis of granitoids here from 160 to 60 Ma. Crustal assimilation alone cannot produce the high Ba/Zr and elevated δ^{18}O values, but a combination of sediment, continental crust, and altered oceanic crust can.

Evidence for the initiation of subduction erosion in the Mexican arc in the Laramide has been recognized previously (e.g., Schaaf et al. 1995). Further south in the Sierra Madre del Sur near Acapulco and Puerto Escondido, the
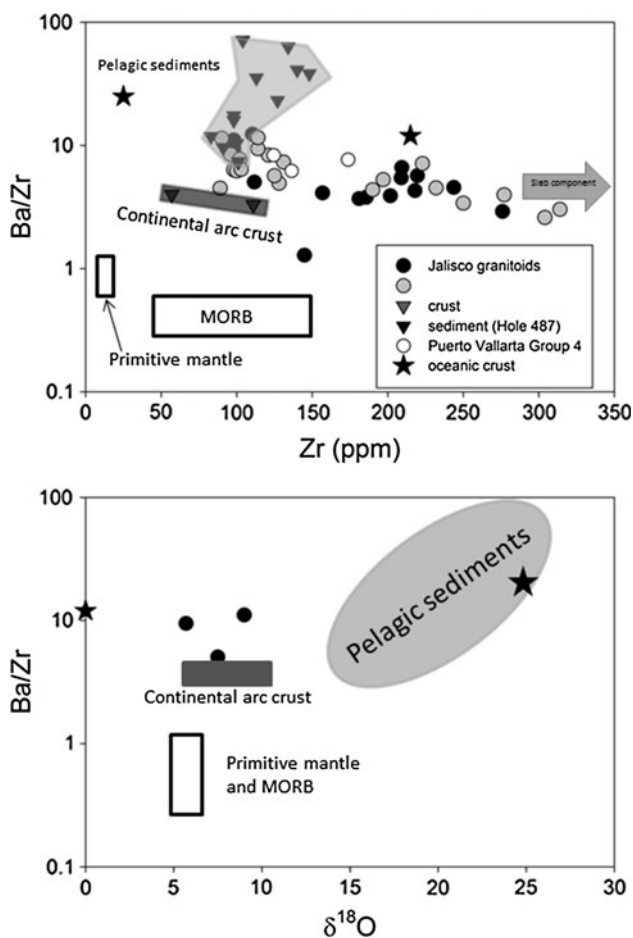
Fig. 10 Oxygen isotope ($\delta^{18}O$) versus Ba/Zr for granitoid samples from the Jalisco Block. Fields labeled "primitive mantle" and "MORB" are based on Ba/Zr values from Lehnert et al. (2000) and oxygen isotopic values from Valley et al. (1998); "continental arc crust" is defined by Ba/Zr data from Rudnick and Fountain (1995) and oxygen isotopic studies of crustal materials by Lackey et al. (2005) and Valley et al. (2005). Sediment Ba/Zr values are from LaGatta (2003) and high $\delta^{18}O$ from studies of Savin and Epstein (1970), Kolodny and Epstein (1976), and Arthur et al. (1983). Stars labeled "oceanic crust" in the legend are the values of low $\delta^{18}O$ and high $\delta^{18}O$ altered oceanic crust from Eiler et al. (2005). "Slab component" in top figure refers to the calculated slab component for various primitive basaltic magmas from Mexico from Johnson et al. (2009). Samples labeled "Puerto Vallarta Group 4" are from Schaaf (1990) and Schaaf et al. (2003) and are argued to result from assimilation of old crust due to the Nd isotopic model ages and ε values

shallow subduction angle, the truncation of geologic features along the modern Acapulco trench, and direct seismic and drill hole observations in the trench suggest that subduction erosion is an important process during the evolution of this part of the arc (Schaaf et al. 1995; Morán-Zenteno et al. 1996, 2007; Ducea et al. 2004). In Jalisco, the lack of a sedimentary accretional prism, the presence of truncated granitic rocks along the coast, and inferred high uplift rates suggest subduction erosion in this region as

well. In addition, two large granitic blocks were found offshore from the Manzanillo batholith, along the inner wall of the Acapulco trench and extending seaward (Calmus et al. 1999; Bandy et al. 1999). The evidence presented here for sedimentary and/or oceanic crustal input into the Jalisco Block granitoids does not require subduction erosion but is fully consistent with that possibility.

Cretaceous to Paleocene silicic ash flow tuff—Carmichael ash flow tuff succession

A major geologic feature of the Jalisco Block that was under-appreciated for many years is the widespread occurrence of silicic ash flow tuffs that have been documented in many parts of the Jalisco Block. The first ages from the reconnaissance studies of Gastil et al. (1978) identified these units as older than the extensive Sierra Madre Occidental (SMO) volcanic units to the northwest. Additional dating by Wallace and Carmichael (1989) and Righter et al. (1995) in central Jalisco revealed the larger extent of these units into the interior of the Jalisco Block. Subsequently, samples of this age range were documented toward the Colima area (Atemajac) by Rosas-Elguera et al. (1997) and to the northwest near Amado Nervo by Frey et al. (2004). Our sample from near Union de Tula (AUT-02) extends the presence of this unit further south near Autlan. Altogether, this unit distinguishes the Jalisco Block from the northern SMO volcanic units, and is a defining geologic characteristic of this part of the Guerrero terrane. The lithologies present in this unit are variable, and can include welded tuffs, crystal tuffs, and lithic tuffs, volcanic breccias, and tuff breccias (see examples in Online Resource 1). The tuffs contain block, lapilli, and ash-sized particles, and overall composition varies from andesitic to rhyolitic (Fig. 4). The age range of the units within this succession is quite wide with some as young as 58 Ma and as old as 83 Ma; a 25-Ma span that indicates the temporal importance of this volcanic unit. In honor of the role that Ian S.E. Carmichael played in the documentation and establishment of the significance of this unit to the geologic history of the region, we propose naming the unit "Carmichael silicic ash flow tuff volcanic succession." It was a favorite topic of Dr. Carmichael's and one that he impressed upon many students of Mexican geology through discussion and field work over several decades.

One outstanding question about the Carmichael tuff is the relation between the Cretaceous age plutons and volcanic rocks in the Jalisco Block. The contact between these units may reveal important information about the geologic history, yet it has not been well documented in studies to date. This could be a fruitful area of investigation in the future studies.

Sources of detrital zircons in Jalisco Block metasediments and schists

Detrital zircons from the sedimentary rocks and phyllitic schists near San Sebastián and Mascota yield a wide range of ages, with most defining peaks at 131 or 140 Ma. However, there are many older Proterozoic and Phanerozoic ages as well, such as 1.7–3.1 Ga. All of these Proterozoic ages could come from a local source in continental Mexico, such as through the Arteaga Complex or the Potosí fan (Centeno-García et al. 2008, 2011). There are other potential sources located further to the north such as Precambrian crust in North America, or the Arizona or Sonora crustal provinces (e.g., Gross et al. 2000; Hawkins and Bowring 1997). However, these sources are much farther away and considered less likely to be represented in the Jalisco units, especially since there are more viable local sources. Finally, there are a significant number of ages between 900 and 1,300 Ma as well as 500–800 Ma, that could represent material from Mexican terranes such as Oaxaquia and Maya, respectively (Centeno-García et al. 2008; Talavera-Mendoza et al. 2005, 2007).

Detrital zircons from the seven schist samples yield more uniform ages, from 135 to 240 Ma, with the older ages similar to those recorded in the Arteaga schist in the eastern Zihuatanejo terrane (Talavera-Mendoza et al.

2007). Additionally, there are some older ages found in the Cuale, Ahuacatlán, and Yelapa samples. The Cuale samples yield four different ages, albeit with a small number of zircons (6); ~650, ~900, ~1,400 and ~1,680 Ma. There are a few zircon ages near 1,100–1,200 Ma for the Ahuacatlán samples, and there are a significant number of zircon ages between 240 and 1,600 Ma in the Yelapa sample. As with the sedimentary rocks, these older ages could represent material from Late Proterozoic or Phanerozoic Mexican units or terranes such as the Potosí fan, Oaxaquia, and Mixteca, respectively (Centeno-García et al. 2008; Talavera-Mendoza et al. 2005, 2007).

All of these older ages in the sedimentary rocks and schists indicate that material comprising these units was derived from continental Mexico and North America and thus from close proximity to a continental shoreline. In fact, the Triassic ages in the Yelapa sample (PV-7) are very similar to those reported in the Arteaga schist in the eastern Zihuatanejo terrane suggesting that this western part of the terrane has a similarly old component, or was linked to the eastern basement units for some time, rather than relatively new terrane material added from an oceanic setting.

The Proterozoic ages in the Jalisco Block zircons could also be explained by the presence of a sliver of old crust in the pre-Cenozoic basement. Schaaf et al. (1995, 2003) argued that the negative epsilon Nd values and 1.2 Ga

model ages calculated for some granitoids from the Jalisco Block suggest the presence of Proterozoic age crust beneath the Puerto Vallarta batholith. Furthermore, Os isotopic analyses of Plio-Quaternary basaltic rocks from the western Mexican volcanic belt, including many from within the Jalisco Block, are radiogenic (0.25–0.4 $^{187}Os/^{188}Os$) indicating a role for assimilation of old crust (Righter et al. 2002; Chesley et al. 2002). Proterozoic age crust could also provide a source of radiogenic Os that is involved in assimilation by basaltic magmas in Jalisco (Righter et al. 2002; Chesley et al. 2002).

Relation of Jalisco Block basement to the rest of the Guerrero terrane

The dominant range of ages of the detrital zircons from schists and sediments and several magmatic zircons falls within the Early Cretaceous to Late Triassic, from 135 to 240 Ma. This age range is very similar to zircon ages from samples from a number of different locations within both the northern Guerrero terrane (El Arco granodiorite porphyry—164 Ma; Valencia et al. 2006; San Pedro Martir orthogneiss and tonalite—$\sim$164 Ma; Schmidt 2000 and Schmidt and Paterson 2002; Punta Norte Cedros Island granitoids—$\sim$163–167 Ma; Kimbrough and Moore 2003) and in the southern Guerrero Terrane (El Fuerte (Sinaloa) granitic plutons and sill—$\sim$155 Ma; Vega-Granillo et al. 2008; southern Sinaloa—134 to 139 Ma; Henry et al. 2003; Arperos Basin—131–151 Ma; Martini et al. 2011; Cuale VMS district in Jalisco—156–162 Ma; Schaaf et al. 2003; Bissig et al. 2008; Mortensen et al. 2008; Tumbiscatío granitoid—164 Ma; Centeno-García et al. 2003; Fig. 11). All of these ages define a fairly narrow time frame, but a very wide area that defines the extent of the Guerrero terrane and equivalents. These Late Jurassic ages for magmatic samples (Cuale and Ahuacatlán) define active magmatism and associated metamorphism in a broad band from Alisitos in the north (Busby et al. 2006) to Zihuatanejo in the south (Centeno-Garcia et al. 2008, 2011). The Jurassic age schists and metasediments of the Jalisco Block were either part of the Jurassic age arc system that is present from North America (Tosdal et al. 1989) all the way south into Mexico (Bartolini 1998), or shed off of that system to form metasediments.

### The role of the Guerrero terrane in the evolution of SW Mexico

The ages of pre-Cenozoic basement units of the Jalisco Block have been largely unknown prior to this study. Early maps showed the presence of pre-Cenozoic crystalline basement of unknown specific age (Gastil et al. 1978). Some maps have even shown this region to be covered by
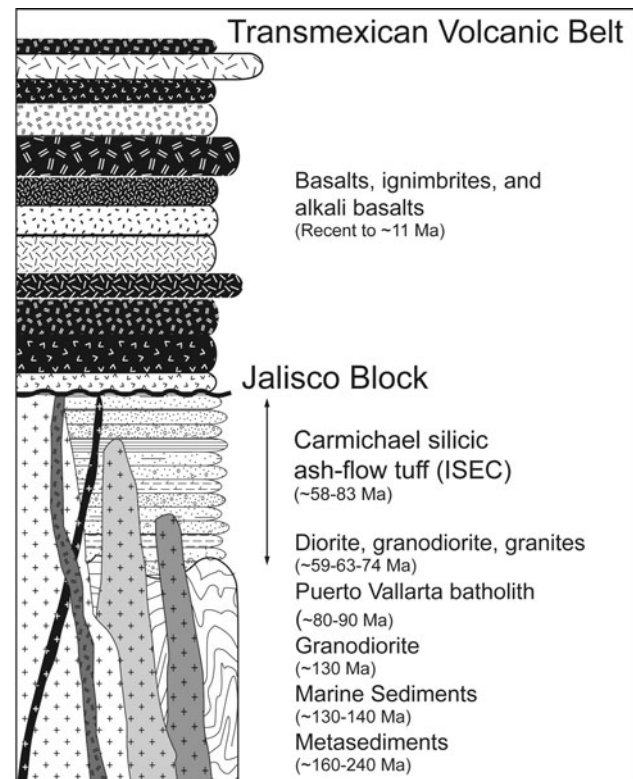
Fig. 12 Stratigraphic column for Jalisco Block, updated with new ages from this study, showing the oldest units from 240 to 160 Ma metasediments (schists from Yelapa, Destiladera, Ahuacatlán, Uzeta, Mascota, and Cuale), to $\sim$130–140 Ma marine sediments (near San Sebastián and Mascota), $\sim$130 Ma granitoid (Ahuacatlán), the $\sim$80–90-Ma age Puerto Vallarta batholith, the 59–74-Ma intrusive suite (from Atenguillo valley), and the 58–83-Ma silicic volcanic ash flow tuff, all of which is overlain by the younger Sierra Madre Occidental and younger units

Cenozoic Sierra Madre Occidental material (Ortega-Gutiérrez et al. 1992; Centeno-García et al. 2008). More recently, Ferrari et al. (2000) indicate that the oldest units in this region are the 114-Ma Puerto Vallarta batholiths, and marine sediments. Centeno-García et al. (2008) show only the Tumbiscatío granitoid and Cuale units in the Jurassic age basement of the Guerrero composite terrane. Our new results for samples from the basement of the Jalisco Block indicate that the western Zihuatanejo terrane (Fig. 1) contains units as old as Triassic and a diversity of Jurassic units beneath the Jalisco region. An updated stratigraphic column for the Jalisco Block is presented in Fig. 12. The Triassic detrital zircon ages in the Yelapa schist overlap with the ages of the Arteaga Complex and Potosí fan further to the east and southeast (Martini et al. 2011; Centeno-García et al. 2011). The Jurassic to Early Cretaceous ages of schists and sediments in the Jalisco Block overlap with the ages of basement units in the Huetamo region of the Zihuatanejo terrane, and similar ages make up the oldest units in the Arcelia and Teloloapan

Fig. 13 Cartoon of evolution of margin of western Mexico in the Jalisco region, from Permian to Paleocene. **a** In the Permo-Triassic, sediments were shed off of the passive continental Mexico to the west, as shown by the 240 Ma and older detrital zircon ages in the Yelapa sample south of Puerto Vallarta. **b** In the Triassic, this boundary was transformed into a subduction zone, at the edge of continental Mexico (ages recorded in the Cuale granitoid and Punta Mita schist samples). **c** This arc system persisted into the Jurassic and Early Cretaceous (Ahuacatlán schist and San Sebastián metasediments) as part of the Mexican Jurassic arc system (see text for discussion). **d** By Late Cretaceous, the island arc was subducted onshore and accreted to North America (∼80-Ma age granitoids in the greater Puerto Vallarta (Tomatlán, El Tuito, Chacala, Punta Mita) area and 61–92 Ma tuffs). Subduction angle of the oceanic plate beneath continental Mexico shallowed in the Late Cretaceous and Early Paleocene, pushing magmatism slightly eastward, where younger (59–63 Ma) plutons and tuffs are found in the Atenguillo, Zacatongo and Amatlán de Cañas area
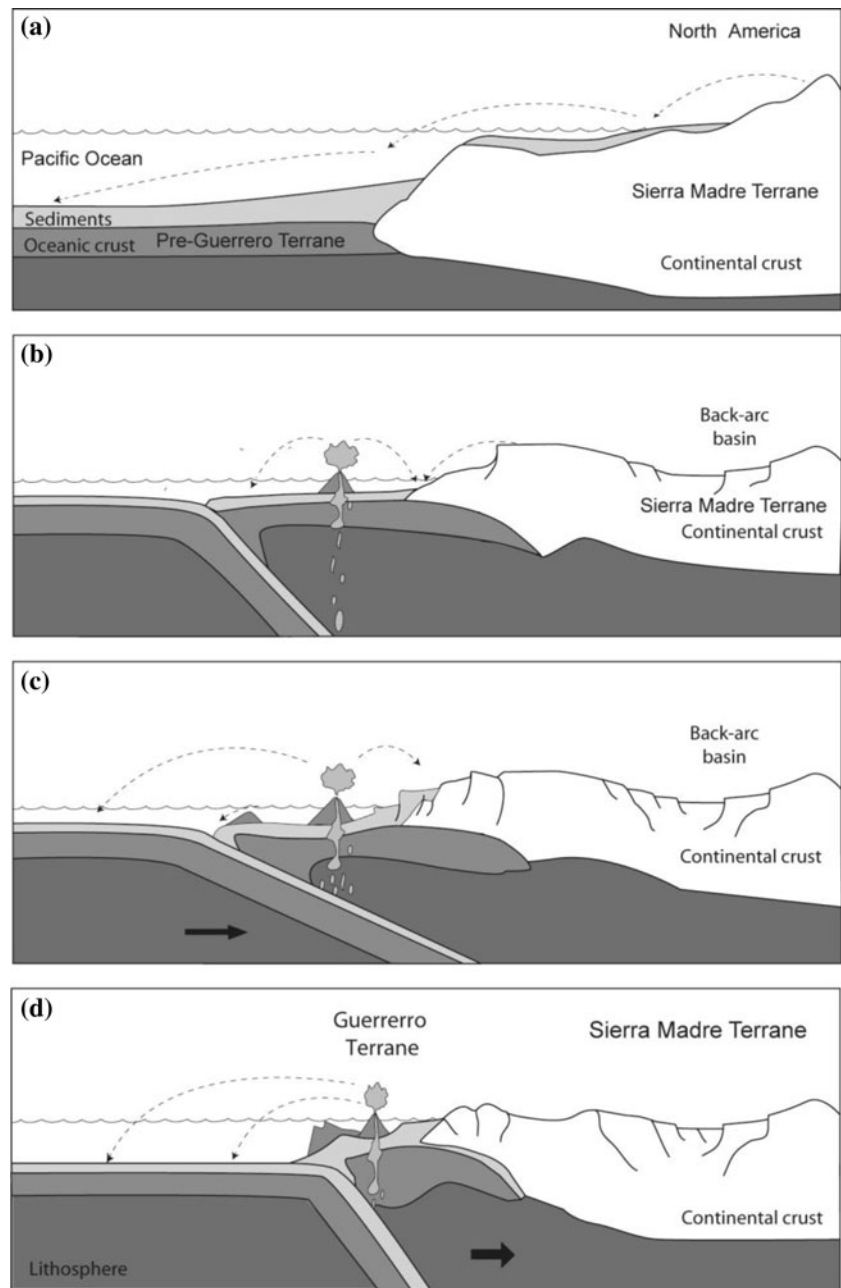
terranes further east in the Guerrero composite terrane (Centeno-García et al. 2008). All of these observations demonstrate that the basement in the Jalisco region is as old as other parts of the Guerrero composite terrane and is undoubtedly part of the Zihuatanejo terrane. This is perhaps not unexpected but here we have provided the missing chronologic link.

The chronologic information reported here allows a more detailed understanding of the evolution of western Mexico, and we can evaluate the two kinds of models for the tectonic evolution of this region: (a) the Guerrero terrane formed from a number of smaller allochthonous (or exotic) terranes accreted to western Mexico (e.g., Dickinson and Lawton 2001; Talavera-Mendoza et al. 2007) or (b) the Guerrero terrane formed from more localized rifting and/or re-accretion of continental material derived mainly from the Mexican continent (Centeno-García et al. 2011; Martini et al. 2011).

Our studies have revealed a significant population of detrital zircons of Paleozoic to Proterozoic age, which at face value is inconsistent with an exotic oceanic origin of these magmas. There could have been localized movement of continental material through a discontinuous volcanic arc, but that seems unlikely. A more likely explanation for

the older zircons is that they were derived from close to the coast of Mexico, and more specifically from the Paleozoic and Proterozoic-aged terranes to the east of the Guerrero terrane. Evidence for Permo-Triassic continental basin sediments is provided by the 240 Ma and older detrital zircon ages in the Yelapa sample south of Puerto Vallarta, as well as Los Cabos and Isla Cerralvo samples. These sediments were shed off of the passive continental margin of Mexico to the west where future Guerrero terrane sediments accumulated (Fig. 13a). Evidence for the Jurassic arc phase is seen in the detrital ages recorded in the Cuale granitoid and Punta Mita schist samples ($\sim$160 Ma) and as late as early Cretaceous as seen in the Ahuacatlán schist and San Sebastián metasediments ($\sim$130 Ma) (Fig. 13b). Amalgamation with the continent was complete by early Cretaceous, as has also been shown for Alisitos to the north (Busby et al. 1998). A continental arc phase is recorded in the $\sim$80-Ma age granitoids and volcanic tuffs in the greater Puerto Vallarta (Tomatlán, El Tuito, Chacala, Punta Mita) and Jalisco Block areas, respectively (Fig. 13c). Possible plate shallowing could have produced a younger band of magmatism further east, where younger (59–63 Ma) plutons and tuffs are found in the Atenguillo, Zacatongo, Amatlán (this study), and Zacoalco (Allan 1986) areas (Fig. 13d).

Conclusions

Whole rock major and trace element analysis, Ar–Ar age dating, U–Pb zircon age dating, and O isotopic analyses of zircons from samples of pre-Cenozoic basement of the Jalisco Block have revealed new information about the geologic and tectonic history of the western margin of Mexico. Specifically, Jalisco granitoids yield cooling rates of 34–48 °C/Ma. The granitoids and volcanic rocks overlap in age and are subalkaline to calc-alkaline in composition, consistent with origin in a convergent margin setting. Prominent geologic units in the pre-Cenozoic Jalisco Block are silicic ash flow tuffs ranging in age between 58 and 83 Ma. Professor Carmichael and his research group noted the widespread occurrence and significance of these tuffs during research in Mexico starting in the 1980s. Because of his interest in this fundamental geologic unit, and its impact on understanding the geologic history of SW Mexico, we propose naming the unit "Carmichael silicic ash flow tuff volcanic succession." Ages of detrital zircons from schists and metasedimentary rocks from the Jalisco Block basement illustrate an origin from continental Mexico, consistent with an autochthonous origin for the western Guerrero terrane rather than an exotic or island arc origin. The Jalisco Block basement units are part of, or were derived from, the Mexican Jurassic arc.

References

Aguirre-Diaz GJ, McDowell FW (1991) The volcanic section at Nazas, Durango, Mexico, and the possibility of widespread Eocene volcanism within the Sierra Madre Occidental. J Geophys Res 96:13373–13388

Allan JF (1986) Geology of the northern Colima and Zacoalco grabens, southwest Mexico: Late Cenozoic rifting in the Mexican Volcanic Belt. Geol Soc Am Bull 97:473–485

Allan JF, Nelson SA, Luhr JF, Carmichael ISE, Wopat M, Wallace PJ (1991) Pliocene—recent rifting in SW Mexico and associated volcanism: an exotic terrane in the making. In: Dauphin JP, Simoneit BRT (eds) The Gulf and Peninsular Province of the Californias: Am Assoc Petrol Geol Mem 47:425–445

Arthur MA, Anderson TF, Kaplan IR (1983) Stable isotopes in sedimentary geology. Soc Econ Pet Mineral Short Course 10, p 432

Bandy WL, Hilde TWC (1995) The subducted Rivera-Cocos Plate Boundary: where is it, what is it, and what is its relationship to the Colima Rift? Geophys Res Lett 22:3075–3078

Bandy W, Kostoglodov V, Hurtado-Diaz A, Mena M (1999) Structure of the southern Jalisco zone, Mexico, as inferred from gravity and seismicity. Geofis Inter 38:127–136

Barrier E, Bourgois J, Michaud F (1990) Le systeme de rifts actifs du point triple de Jalisco: vres un proto-golfe de Jalisco. Comte Rend Acad Sci II 310:1513–1520

Bartolini C (1998) Stratigraphy, geochronology, geochemistry and tectonic setting of the Mesozoic Nazas Formation, north-central México. Unpub Ph.D. thesis, University of Texas, El Paso, p 558

Bissig T, Mortensen JK, Tosdal RM (2008) The rhyolite-hosted volcanogenic massive sulfide District of Cuale, Guerrero terrane, West-Central Mexico: silver-rich, base metal mineralization emplaced in a shallow marine continental margin setting. Econ Geol 103:141–159

Böhnel H, Negendank JFW (1988) Palaeomagnetism of the Puerto Vallarta intrusive complex and the accretion of the Guerrero terrain, Mexico. Phys Earth Planet Inter 52:330–338

Böhnel H, Moran-Zenteno D, Schaaf P, Urrutia-Fucugauchi J (1992) Paleomagnetic and isotopic data from southern Mexico and the controversy over the pre-Neogene position of Baja California. Geof Intern 31:253–262

Busby C (2004) Continental growth at convergent margins facing large ocean basins: a case study from Mesozoic convergent-

margin basins of Baja California, Mexico. Tectonophysics 392:241–277

Busby C, Smith D, Morris W, Fackler-Adams B (1998) Evolutionary model for convergent margins facing large oceanic basins: mesozoic Baja California, Mexico. Geology 26:227–230

Busby C, Adams B, Mattinson J, Deoreo S (2006) View of an intact oceanic arc, from surficial to mesozonal levels: Cretaceous Alisitos arc, Baja California. J Volcanol Geotherm Res 149:1–46

Calmus T, Poupeau G, Bourgois J, Michaud F, de Lepinay B, Labrin E, Azdimousa A (1999) Late Mesozoic and Cenozoic thermo-tectonic history of the Mexican Pacific margin (18 to 25°N): new insight from apatite and zircon fission-track analysis of coastal and offshore plutonic rocks. Tectonophysics 306:163–182

Campa MF, Coney PJ (1983) Tectono-stratigraphic terranes and mineral resource distributions in Mexico. Can J Earth Sci 20:1040–1051

Centeno-García E, Ruíz J, Coney P, Patchett JP, Ortega GF (1993) Guerrero Terrane of Mexico: its role in the Southern Cordillera from new geochemical data. Geology 21:419–422

Centeno-García E, Corona-Chávez P, Talavera-Mendoza Ó, Iriondo A (2003) Geology and tectonic evolution of the western Guerrero terrane—a transect from Puerto Vallarta to Zihuatanejo, Mexico. In: Geologic transects across Cordilleran Mexico, guidebook for the field trips of the 99th Geological Society of America Cordilleran section annual meeting, Puerto Vallarta, Jalisco, Mexico, 4–6 Apr 2003. Universidad Nacional Autónoma de México, Instituto de Geología, Mexico, D.F., Publicación Especial 1, Field trip 9:201–228

Centeno-García E, Guerrero-Suastegui M, Talavera-Mendoza O (2008) The Guerrero composite terrane of western Mexico: collision and subsequent rifting in a supra-subduction zone. Geol Soc Am Spec Pap 436:279–308

Centeno-García E, Busby C, Busby M, Gehrels G (2011) Evolution of the Guerrero composite terrane along the Mexican margin, from extensional fringing arc to contractional continental arc. Geol Soc Am Bull 123:1776–1797

Chang Z, Vervoort JD, McClelland WC, Knaack C (2006) U–Pb dating of zircon by LA-ICP-MS. Geochem Geophys Geosyst 7:Q05009. doi:10.1029/2005GC001100

Cherniak DJ, Watson EB (2001) Pb diffusion in zircon. Chem Geol 172:5–24

Chesley JT, Ruiz J, Righter K, Ferrari L, Gomez-Tueno A (2002) Source contamination versus assimilation: an example from the Trans-Mexican volcanic arc. Earth Planet Sci Lett 195:211–221

Corfu F, Hanchar JM, Hoskin PWO, Kinny PD (2003) Atlas of zircon textures (in Zircon). Rev Mineral Geochem 53:469–500

DeMets C, Traylen S (2000) Motion of the Rivera Plate since 10 Ma relative to the Pacific and North American plates and the mantle. Tectonophysics 318:119–159

Dickinson WR, Lawton TF (2001) Carboniferous to Cretaceous assembly and fragmentation of Mexico. Geol Soc Am Bull 113:1142–1160

Dodson MH (1973) Closure temperature in cooling geochronological and petrological systems. Contrib Mineral Petrol 40:259–274

Dougherty SL, Clayton RW, Helmberger DV (2012) Seismic structure in central Mexico: implications for fragmentation of the subducted Cocos Plate. Geophys Res Lett 117:B09316. doi:10.1029/2012JB009528

Ducea MN, Valencia VA, Shoemaker S, Reiners PW, DeCelles PG, Campa MF, Morán-Zenteno D, Ruiz J (2004) Rates of sediment recycling beneath the Acapulco trench: constraints from (U–Th)/He thermochronology. J Geophys Res 109:B09404. doi:10.1029/2004JB003112

Eiler JM, Carr JM, Reagan M, Stolper E (2005) Oxygen isotope constraints on the sources of Central American arc lavas. Geochem Geophys Geosyst 6:Q07007. doi:10.1029/2004GC000804

Ferrari L, Rosas-Elguera J (2000) Late Miocene to Quaternary extension at the northern boundary of the Jalisco block, western Mexico: the Tepic-Zacoalco rift revised. In: Delgado-Granados H, Aguirre-Diaz G, Stock J (eds) Cenozoic tectonics and volcanism of Mexico. Geol Soc Am Bull Spec Pap 334:41–64

Ferrari L, Nelson SA, Rosas-Elguera J, Aguirre-Diaz GJ, Venegas-Salgado S (1997) Tectonics and volcanism of the western Mexican Volcanic Belt. In: Aguirre-Diaz GJ, Aranda-Gomez JJ, Carrasco-Nunez G, Ferrari L (eds) Magmatism and tectonics in central and northwest Mexico—a selection of the 1997 IAVCEI general assembly excursions. UNAM Instituto de Geologia, Mexico, D.F., excursion 12:85–129

Ferrari L, Pasquaré G, Venegas S, Romero F (2000) Geology of the western Mexican Volcanic Belt and adjacent Sierra Madre Occidental and Jalisco block. In: Delgado-Granados H, Aguirre-Diaz G, Stock J (eds) Cenozoic tectonics and volcanism of Mexico. Geol Soc Am Bull Spec Pap 334:64–83

Ferrari L, Valencia-Moreno M, Bryan S (2007) Magmatism and tectonics of the Sierra Madre Occidental and its relation with the evolution of the western margin of North America. Geol Soc Am Spec Pap 422:1–39

Frey HM, Lange RA, Hall CM, Delgado-Granados H (2004) Magma eruption rates constrained by $^{40}Ar/^{39}Ar$ chronology and GIS for the Ceboruco-San Pedro volcanic field, western Mexico. Geol Soc Am Bull 166:259–276

Frey HM, Lange RA, Hall CM, Delgado-Granados H, Carmichael ISE (2007) A Pliocene ignimbrite flare-up along the Tepic-Zacoalco Rift: evidence for the initial stages of rifting between the Jalisco Block (Mexico) and North America. Geol Soc Am Bull 119:49–64

Frost BR, Barnes CG, Collins WJ, Arculus RJ, Ellis DJ, Frost CD (2001) A geochemical classification for granitic rocks. J Petrol 42:2033–2048

Gastil G, Krummenacher D, Jensky WA (1978) Reconnaissance geology of west-central Nayarit, Mexico: Geological Society of America Map and Chart Series MC-24, map 1:200,000

Gehrels G, Valencia VA, Ruiz J (2008) Enhanced precision, accuracy, efficiency, and spatial resolution of U–Pb ages by laser ablation-multicollector-inductively coupled plasma-mass spectrometry. Geochem Geophys Geosyst 9(3). doi:10.1029/2007GC001805

Govindaraju K (1994) Compilation of working values and sample descriptions for 383 geostandards. Geostand Newsl Spec Issue 18:15–53

Gross EA, Stewart JH, Gehrels G (2000) Detrital zircon geochronology of Neoproterozoic to middle Cambrian miogeoclinal and platformal strata, northwest Sonora, Mexico. Geofis Inter 39:295–308

Hawkins DP, Bowring SA (1997) U–Pb systematics of monazite and xenotime: case studies from the Paleoproterozoic of the Grand Canyon, Arizona. Contrib Mineral Petrol 127:87–103

Henry CD, McDowell FW, and Silver LT (2003) Geology and geochronology of granitic batholithic complex, Sinaloa, México: Implications for Cordilleran magmatism and tectonics. In: Johnson SE, Paterson SR, Fletcher JM, Girty GH, Kimbrough DL, Martín-Barajas A (eds) Tectonic evolution of Northwestern México and the Southwestern USA: Geological Society of America Special Paper 374:237–274

Johnson DM, Hooper PR, Conrey RM (1999) XRF analysis of rocks and minerals for major and trace elements on a single low dilution Li-tetraborate fused bead. Adv X-Ray Anal 41:843–867

Johnson E, Wallace PJ, Delgado-Granados H, Manea VC, Kent AR, Bindemann I, Donegan CS (2009) Subduction-related volatile recycling and magma generation beneath central Mexico: insights from melt inclusions, oxygen isotopes and geodynamic models. J Petrol 50:1729–1754

Jones NW, McKee JW, Anderson TH, Silver LT (1995) Jurassic volcanic rocks in northeastern Mexico: a possible remnant of a

Cordilleran magmatic arc. In: Jacques-Ayala C, González-León CM, Roldán-Quintana J (eds) Studies on the Mesozoic of Sonora and adjacent areas. Boulder, Colorado, Geol Soc Amer Spec Pap 301:179–190

Kimbrough DL, Moore TH (2003) Ophiolite and volcanic arc assemblages on the Vizcaıno Peninsula and Cedros Island, Baja California Sur, Meʹxico: Mesozoic forearc lithosphere of the Cordilleran magmatic arc. In: Johnson SE, Paterson SR, Fletcher JM, Girty GH, Kimbrough DL, Martıʹn-Barajas A (eds) Tectonic evolution of northwestern Mexico and the southwestern USA. Geol Soc Am Spec Pap 374:43–71

Köhler H, Schaaf P, Müller-Sohnius D, Emmerman R, Negendank JFW, Tobschall HJ (1988) Geochronological and geochemical investigations on plutonic rocks from the complex of Puerto Vallarta, Sierra Madre del Sur. Geofis Inter 27:519–542

Kolodny Y, Epstein S (1976) Stable isotope geochemistry of deep sea cherts. Geochim Cosmochim Acta 40:1195–1209

Lackey JS, Valley JW, Saleeby JB (2005) Supracrustal input to magmas in the deep crust of Sierra Nevada batholith: evidence from high-$\delta^{18}O$ zircon. Earth Planet Sci Lett 235:315–330

LaGatta A (2003) Arc magma genesis in the eastern Mexican volcanic belt. Ph.D. thesis, Columbia University, New York

Lange RA, Carmichael ISE (1991) A potassic volcanic front in western Mexico: the lamprophyric and related lavas of San Sebastían. Geol Soc Am Bull 103:928–940

Le Bas MJ, Streckeisen AL (1991) The IUGS systematics of igneous rocks. J Geol Soc Lond 148:825–833

Lehnert K, Su Y, Langmuir CH, Sarbas B, Nohl U (2000) A global geochemical database structure for rocks. Geochem Geophys Geosyst 1(5). doi:10.1029/1999GC000026

Lonsdale P (1995) Segmentation and disruption of the East Pacific Rise in the Mouth of the Gulf of California. Mar Geophys Res 17:323–355

Ludwig KR (2003) Isoplot 3.00: Berkeley, CA, Berkeley Geochronology Center Special Publication No. 4, p 70

Luhr JF (1997) Extensional tectonics and the diverse primitive volcanic rocks in the western Mexican Volcanic Belt. Can Mineral 35:473–500

Luhr JF, Nelson SA, Allan JF, Carmichael ISE (1985) Active rifting in southwestern Mexico: manifestations of an incipient eastward spreading ridge jump. Geology 13:54–57

Martini M, Mori L, Solari L, Centeno-García E (2011) Sandstone provenance of the Arperos Basin (Sierra de Guanajuato, central Mexico): Late Jurassic–Early Cretaceous back-arc spreading as the foundation of the Guerrero terrane. J Geol 119:597–617

McDowell FW, Keizer RP (1977) Timing of mid-Tertiary volcanism in the Sierra Madre Occidental between Durango City and Mazatlan, Mexico. Geol Soc Am Bull 88:1479–1487

Moore G, Marone C, Carmichael ISE, Renne P (1994) Basaltic volcanism and extension near the intersection of the Sierra Madre volcanic province and the Mexican Volcanic Belt. Geol Soc Am Bull 106:383–394

Morán-Zenteno DJ, Corona-Chavez P, Tolson G (1996) Uplift and subduction erosion in southwestern Mexico since the Oligocene: pluton geobarometry constraints. Earth Planet Sci Lett 141: 51–65

Morán-Zenteno DJ, Cerca M, Keppie JD (2007) The Cenozoic tectonic and magmatic evolution of southwestern México: advances and problems of interpretation. In: Alaniz-Álvarez SA, Nieto-Samaniego ÁF (eds) Geology of México: Celebrating the Centenary of the Geological Society of México: Geological Society of America Special Paper 422:71–91. doi:10.1130/2007.2422(03).

Mortensen JK, Ball BV, Bissig T, Friedman RM, Danileson T, Oliver J, Rhys DA, Ross KV, Gabites JE (2008) Age and paleotectonic setting of volcanogenic massive sulphide deposits in the Guerrero terrane of central Mexico: constraints from U–Pb age and Pb isotopic studies. Econ Geol 103:117–140

Ortega-Gutiérrez F, Mitre-Salazar LM, Roldán-Quintana J, Aranda-Gómez JJ, Morán-Zenteno DJ, Alaniz-Álvarez SA, Nieto-Samaniego ÁF (1992) Carta geológica de la República Mexicana, quinta edición escala 1:2,000,000: México, D. F., Universidad Nacional Autónoma de México, Instituto de Geología; Secretaría de Energía, Minas e Industria Paraestatal, Consejo de Recursos Minerales, 1 sheet

Pearce JN, Harris NBW, Tindle A (1984) Trace element discrimination diagrams for the tectonic interpretation of granitic rocks. J Petrol 25:956–983

Renne PR, Swisher CC, Deino AL, Karner DB, Owens TL, DePaolo DJ (1998) Intercalibration of standards, absolute ages and uncertainties in $^{40}Ar/^{39}Ar$ dating. Chem Geol 145:117–152

Righter K (2000) A comparison of basaltic volcanism in the Cascades and western Mexico: compositional diversity in continental arcs. Tectonophysics 318:99–117

Righter K, Carmichael ISE (1992) Hawaiites and related lavas in the Atenguillo graben, western Mexican Volcanic Belt. Geol Soc Am Bull 104:1592–1607

Righter K, Carmichael ISE, Becker TA, Renne RP (1995) Pliocene to Quaternary volcanism and tectonism at the intersection of the Mexican Volcanic Belt and the Gulf of California. Geol Soc Am Bull 107:612–626

Righter K, Chesley JT, Ruiz J (2002) Genesis of primitive arc-type basalt: constraints from Re, Os and Cl on the depth of melting and role of fluids. Geology 30:619–622

Righter K, Valencia V, Rosas-Elguera J, Caffee M (2010) Channel incision in the Rio Atenguillo, Jalisco, Mexico: ^{36}Cl constraints on rates and cause. Geomorphology 120:279–292

Rosas-Elguera J, Nieto-Obregón J, Urrutia-Fucugauchi J (1993) Ambiente estructural en la frontera Norte del bloque Jalisco. In: Delgado-Argote L, Martin-Barajas A (eds) Contribuciones a la Tectónica del Occidente de México, Unión GeofÌsica Mexicana 1:175–192

Rosas-Elguera J, Ferrari L, Garduño VH, Urrutia-Fucugauchi J (1996) The continental boundaries of the Jalisco block and their influence in the Plio-Quaternary kinematics of western Mexico. Geology 24:921–923

Rosas-Elguera J, Ferrari L, López-Martinez M, Urrutia-Fucugauchi J (1997) Stratigraphy and tectonics of the Guadalajara region and the triple junction area, western Mexico. Int Geol Rev 39:125–140

Rudnick RL, Fountain D (1995) Nature and composition of the continental crust: a lower crustal perspective. Rev Geophys 33:267–309

Savin SM, Epstein S (1970) The oxygen and hydrogen isotope geochemistry of ocean sediments and shales. Geochim Cosmochim Acta 34:43–57

Schaaf P (1990) Isotopengeochemische Untersuchungen an granitoiden Gesteinen eines aktiven Kontinentalrandes: Alter und Herkunft der Tiefengesteinskomplexe an der Pazifikküste Mexikos zwischen Puerto Vallarta und Acapulco. PhD Thesis, University of Munich, Germany, p 202

Schaaf P, Morán-Zenteno D, del Sol Hernández-Bernal M, Solís-Pichardo G, Tolson G, Köhler H (1995) Paleogene continental margin truncation in southwestern Mexico: geochronological evidence. Tectonics 14:1339–1350

Schaaf P, Böhnel H, Pèrez-Venzor JA (2000) Pre-Miocene palaeogeography of the Los Cabos Block, Baja California Sur: geochronological and palaeomagnetic constraints. Tectonophysics 318:53–69

Schaaf P, Hall BV, Bissig T (2003) The Puerto Vallarta Batholith and Cuale Mining District, Jalisco, Mexico—high diversity parenthood of continental arc magmas and Kuroko-type volcanogenic

massive sulphide deposits. In: Geologic transects across cordilleran Mexico, guidebook for field-trips of the 99th annual meeting of the Cordilleran section of the Geological Society of America, Mexico, D. F., 31 Mar 2003: Universidad Nacional Autónoma de México, Instituto de Geología, Publicación Especial 1, Field trip 8:183–199

Schmidt KL (2000) Investigation of arc processes: relationships among deformation, magmatism, mountain building, and the role of crustal anisotropy in the evolution of the Peninsular Ranges batholith, Baja California, Ph.D. thesis, p 310, Univ. of S. Calif., Los Angeles

Schmidt KL, Paterson SR (2002) A doubly vergent fan structure in the Peninsular Ranges batholith: transpression or local complex flow around a continental margin buttress? Tectonics 21:1050–1062. doi:10.1029/2001TC001353

Sedlock RL, Ortega-Gutierrez F, Speed RC (1993) Tectonostratigraphic Terranes and tectonic evolution of Mexico. Geol Soc Am Spec Pap 278:153

Slodzian G (1980) Microanalyzers using secondary ion emission. In Advances in electronics and electron physics 138. Academic Press suppl., 1–44

Spinnler J, Garduno VH, Ceragioli E (2000) Stratigraphic and structural relations between the trans-Mexican volcanic belt and the Sierra Madre Occidental in the Guadalajara region, Jalisco, Mexico. In: Delgado-Granados H, Aguirre-Diaz G, Stock J (eds) Cenozoic tectonics and volcanism of Mexico. Geol Soc Amer Bull Spec Pap 334:85–97

Steiger RH, Jager E (1977) Subcommision on geochronology: convention on the use of decay constants in geo and cosmochronology. Earth Planet Sci Lett 36:359–362

Talavera-Mendoza O, Ruiz J, Gehrels GE, Meza-Figueroa DM, Vega-Granillo R, Campa-Uranga MF (2005) U-Pb geochronology of the Acatlan Complex and implication for the Paleozoic paleogeography and tectonic evolution of southern Mexico. Earth Planet Sci Lett 235:682–699

Talavera-Mendoza O, Ruiz J, Gehrels GE, Valencia VA, Centeno-García E (2007) Detrital zircon U/Pb geochronology of southern Guerrero and western Mixteca arc successions (southern Mexico): new insights for the tectonic evolution of southwestern North America during the Late Mesozoic. Geol Soc Am Bull 119:1052–1065

Tepper JH, Nelson BK, Bergantz GW, Irving AJ (1993) Petrology of the Chilliwack batholith, North Cascades, Washington: generation of calc-alkaline granitoids by melting of mafic lower crust with variable water fugacity. Contrib Mineral Petrol 113:333–351

Tosdal RM, Haxel GB, Wright JE (1989) Jurassic geology of the Sonoran Desert region, southern Arizona, southeastern California, and northernmost Sonora: Construction of a continental-margin magmatic arc. In: Jenny JP, Reynolds SJ (eds) Geologic evolution of Arizona. Arizona Geological Society Digest 17:397–434

Valencia V, Ruiz J, Barra F, Gehrels G, Ducea M, Titley S, Ochoa-Landin L (2005) U–Pb zircon and Re–Os molybdenite geochronology from La Caridad porphyry copper deposit: insights for the duration of magmatism and mineralization in the Nacozari District, Sonora, Mexico. Miner Deposita 40:175–191

Valencia VA, Barra F, Weber B, Ruiz J, Gehrels G, Chesley JT, Lopez-Martinez M (2006) Re–Os and U–Pb geochronology of the El Arco porphyry copper deposit, Baja California Mexico: implications for the Jurassic tectonic setting. J S Am Earth Sci 22:39–51

Valley JW, Kinny PD, Schulze DJ, Spicuzza MJ (1998) Zircon megacrysts from kimberlite: oxygen isotope heterogeneity among mantle melts. Contrib Mineral Petrol 133:1–11

Valley JW, Lackey JS, Cavosie AJ, Clechenko CC, Spicuzza MJ, Basei MAS, Bindeman IN, Ferreira VP, Sial AN, King EM, Peck WH, Sinha AK, Wei CS (2005) 4.4 billion years of crustal maturation: oxygen isotope ratios of magmatic zircon. Contrib Mineral Petrol 150:561–580

Vega-Granillo R, Salgado-Souto S, Herrera-Urbina S, Valencia V, Ruiz J, Meza-Figueroa D, Talavera-Mendoza O (2008) U-Pb detrital zircon data of the Rio Fuerte Formation (NW Mexico): its peri-Gondwanan provenance and exotic nature in relation to southwestern North America. J S Am Earth Sci 26:343–354

Wallace P, Carmichael ISE (1989) Minette lavas and associated leucitites from the western front of the Mexican Volcanic Belt: petrology, chemistry and origin. Contrib Mineral Petrol 103:470–492

Wallace P, Carmichael ISE (1992) Alkaline and calc-alkaline lavas near Los Volcanes, Jalisco, Mexico: geochemical diversity and its significance in volcanic arcs. Contrib Mineral Petrol 111:423–439

York D, Evensen NM, Lopez-Martinez M, De Basabe-Delgado J (2004) Unified equations for the slope, intercept, and standards errors of the best straight line. Am J Phys 73:367–375

Zimmerman J-L, Stussi J-M, Gonzalez-Partida E, Arnold A (1988) K–Ar evidence for age and compositional zoning in the Puerto Vallarta—Rio Santiago Batholith (Jalisco, Mexico). J S Am Earth Sci 1:267–274